

Origin of the Powai ankaramite, and the composition, P–T conditions of equilibration and evolution of the primary magmas of the Deccan tholeiites

Nilanjan Chatterjee · Hetu Sheth

Received: 26 August 2014 / Accepted: 20 February 2015
© Springer-Verlag Berlin Heidelberg 2015

Abstract The Powai ankaramite flow from Mumbai, western Deccan Traps, contains abundant crystals of augite ($\text{En}_{59-47}\text{Fs}_{10-14}\text{Wo}_{27-42}$, 22–40 modal %, 3–5 mm) and olivine (Fo_{84-74} , 11–16 modal %, 1–2 mm), and minor plagioclase (An_{71} , ~0.5 mm) embedded in a fine-grained matrix. Minor orthopyroxene ($\text{En}_{79-77}\text{Fs}_{16-19}\text{Wo}_{5-4}$) with irregular and embayed margins is mantled by thick augite overgrowth rims. The Fe–Mg distribution between the large crystals and bulk rock shows disequilibrium, indicating that the ankaramite is a cumulate rock. The ankaramite probably formed by the intrusion of tholeiitic melt into a cumulate pile with olivine, augite, and orthopyroxene left by the crystallization of earlier magmas, resulting in orthopyroxene dissolution and subsequent precipitation of augite. Olivine-hosted melt inclusions and melts represented by the ankaramite groundmass and some associated tholeiitic dikes are multiply saturated with olivine + plagioclase + clinopyroxene at ≤ 6 kb according to phase equilibrium constraints. Calculations involving incremental addition of equilibrium phases to these melts and to the common aphyric tholeiites of the voluminous Ambenali

and Mahabaleshwar Formations show that their primary magmas (wt% SiO_2 : 48–50, MgO: 9.8–11.8, and FeO: 7.2–7.9, and Mg# 70–74) last equilibrated with spinel lherzolite at ~8–13 kb (~30–49 km depths) and ~1268–1332 °C, and trace element considerations indicate ≤ 15 % batch melting of mantle. These tholeiitic primary magmas then underwent olivine gabbro fractionation in upper crustal magma chambers at depths ≤ 23 km. The minimum depth of equilibration of the primary magmas is shallower than the present-day Moho in the Mumbai area based on seismological data, indicating localized mantle upwelling and lower crustal interactions previously inferred from the Nd–Sr isotopic ratios and other geochemical characteristics of the ankaramite and associated tholeiites.

Keywords Deccan Traps · Ankaramite · Tholeiite · Primary magma · Thermobarometry · Mantle melting

Introduction

Estimates of compositions of primary magmas, i.e., magmas in equilibrium with all the minerals in their source mantle, provide important constraints on the composition, potential temperature, pressure–temperature (P–T) conditions of equilibration, and the degree of partial melting of the mantle (Thompson 1975; Farnetani et al. 1996; Takahashi et al. 1998; Green et al. 2001; Courtier et al. 2007; Till et al. 2013). Several studies have attempted to characterize the primary magmas of the Deccan flood basalts in western India (Fig. 1a; Krishnamurthy and Cox 1977; Sen 1988, 1995; Cohen and Sen 1994; Melluso et al. 1995; Sen and Chandrasekharam 2011). Sen (1988) compared primitive Deccan tholeiites with experimental partial melts of peridotite (Takahashi and Kushiro 1983) and concluded

Communicated by Othmar Müntener.

Electronic supplementary material The online version of this article (doi:10.1007/s00410-015-1125-8) contains supplementary material, which is available to authorized users.

N. Chatterjee (✉)
Department of Earth, Atmospheric and Planetary Sciences,
Massachusetts Institute of Technology, Cambridge, MA 02139,
USA
e-mail: nchat@mit.edu

H. Sheth
Department of Earth Sciences, Indian Institute of Technology
Bombay, Powai, Mumbai 400076, India

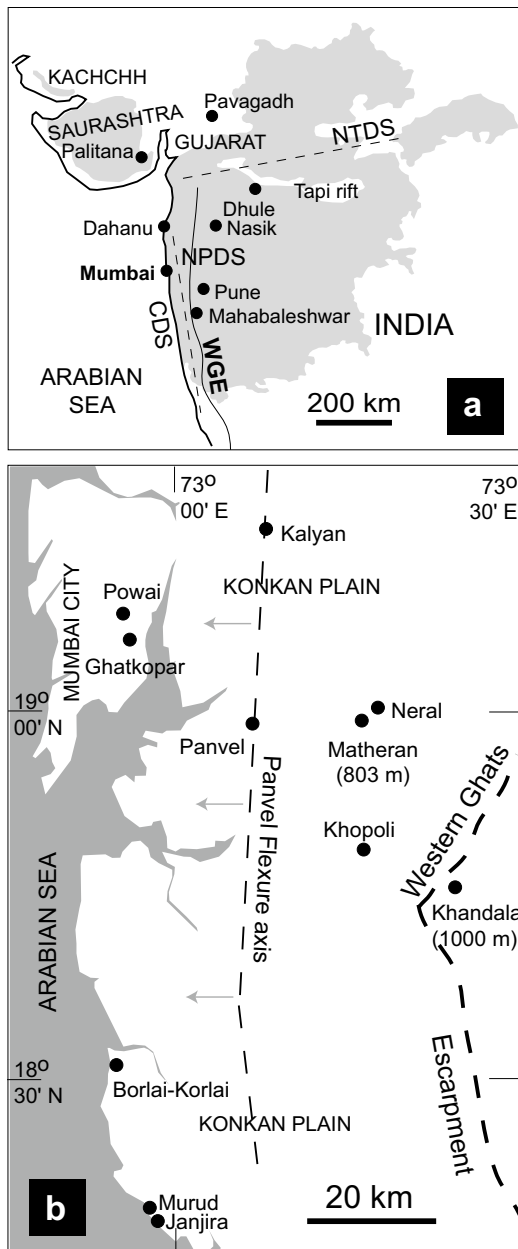


Fig. 1 Maps (after Sheth et al. 2014) of **a** western and central India showing the distribution of the Deccan Traps (gray), and the locations of the Western Ghats escarpment (WGE), the coastal (CDS) and the Narmada–Tapi (NTDS) dike swarms with regional trends (dashed lines), and the Nasik–Pune dike swarm (NPDS); the N–S axis of the Panvel flexure is between the western Indian coast and the WGE, and **b** a part of the western Deccan Traps showing the localities mentioned in the text; gray arrows indicate the westerly dips of the Deccan lava pile west of the Panvel flexure axis

that the aphyric Deccan tholeiites with 9–10 wt% MgO, 9–10 wt% FeO, and molar Mg numbers [$Mg\# = 100 \cdot Mg / (Mg + Fe^{2+})$] of ~64–68 are primary magmas generated at 35–45 km depths. The majority of Deccan tholeiites, however, represent evolved, low-MgO magmas derived

by olivine gabbro (olivine + plagioclase + clinopyroxene) fractionation from primitive tholeiitic liquids in upper crustal magma chambers (Cox 1980; Cox and Hawkesworth 1985; Lightfoot et al. 1990; Cohen and Sen 1994; Sen 1995; Bhattacharji et al. 1996; Sano et al. 2001). Sen (1995) reviewed published data sets and concluded that two compositions with ~7.5 wt% MgO, namely Decc1 (renamed Amb1 by Sen and Chandrasekharam 2011) and Amb2, are parental to the Ambenali and other common Deccan tholeiites of the thick Western Ghats sequence (Fig. 1a). Furthermore, he used Klein and Langmuir's (1987) algorithm to reconstruct mantle olivine (Fo_{90})-equilibrated magma compositions by adding equilibrium olivine to the Ambenali parental magmas. He interpreted these calculated Fo_{90} -equilibrated magmas with 14–15 wt% MgO as the picritic primary magmas of the Ambenali tholeiites. These magmas are also richer in Fe than experimental partial melts of peridotite, a feature attributed by Sen (1995) to melting of Fe-rich mantle peridotite.

Picrites *sensu lato* with >12 wt% MgO (IUGS classification, Le Bas 2000) are common in the Deccan Traps of Gujarat and Saurashtra (Kathiawar) in the northwestern part of the province (Krishnamurthy and Cox 1977; Melluso et al. 1995) as well as in the Western Ghats near the west coast of India (Fig. 1a, Beane et al. 1986; Beane and Hooper 1988; Krishnamurthy et al. 2000). It should be noted that many Deccan picrites in a geochemical sense are petrographically ankaramites containing phenocrysts of olivine and clinopyroxene with the latter more abundant (West 1958; Krishnamacharlu 1972; Krishnamurthy and Cox 1977). A good example of an ankaramite occurs in the Neral Formation of the lower Western Ghats sequence, whose type section is located ~50 km east of Mumbai (Fig. 1b). It consists of abundant olivine phenocrysts and centimeter-sized radial glomerocrysts of clinopyroxene surrounded by a fine-grained matrix (Beane et al. 1986).

Beane and Hooper (1988) concluded that the picrites from the lower Western Ghats sequence showing cumulus enrichment of olivine ($Fo_{<84}$) and clinopyroxene do not represent primitive liquids. On the other hand, high-MgO picrites with Fo_{88-92} olivine from Gujarat and especially from Saurashtra (Fig. 1a) have been interpreted as near-primary liquids with ~16 wt% MgO (Krishnamurthy and Cox 1977; Cox 1980; Melluso et al. 1995, 2006; Krishnamurthy et al. 2000; Sheth and Melluso 2008; Sen and Chandrasekharam 2011). Krishnamurthy and Cox (1977) considered these picrites as parental to the interlayered tholeiites and concluded that the tholeiites evolved through equilibrium crystallization aided by compensated crystal settling from picritic liquids. Melluso et al. (1995) argued that the somewhat alkalic and high-TiO₂ picrites of Saurashtra and Gujarat formed from clinopyroxene-rich mantle sources. They normalized these picrite compositions to 15 wt% MgO by adding equilibrium olivine and

Table 1 Geochemical stratigraphy of the Western Ghats section, Deccan Traps

Group	Subgroup	Formation	Magnetic polarity	$^{87}\text{Sr}/^{86}\text{Sr}_{(65\text{ Ma})}$
Deccan basalt	Wai	Desur ^a (~100 m)	N	0.7072–0.7080
		Panhala (>175 m)	N	0.7046–0.7055
		Mahabaleshwar (280 m)	N	0.7040–0.7055
		Ambenali (500 m)	R	0.7038–0.7044
		Poladpur (375 m)	R	0.7053–0.7110
	Lonavala	Bushe (325 m)	R	0.7078–0.7200
		Khandala (140 m)	R	0.7071–0.7124
	Kalsubai	Bhimashankar (140 m)	R	0.7067–0.7077
		Thakurvadi ^b (650 m)	R	0.7067–0.7224
		Neral (100 m)	R	0.7062–0.7104
		Jawhar–Igatpuri (>700 m)	R	0.7085–0.7128

^a The Desur is considered by many as a “Unit” of the Panhala Formation itself. ^b The Sr isotopic range for most of the Thakurvadi Formation lavas is 0.7067–0.7112, but a single flow in the formation (Paten Basalt) has an anomalously high, broadly Bushe-like value (0.7224). Table based on Subbarao and Hooper (1988) and references therein, Peng et al. (1994), Vanderkluyzen et al. (2011), and Sheth et al. (2014). N = normal magnetic polarity, R = reverse magnetic polarity

used Hirose and Kushiro’s (1993) experimental data to calculate pressures of 11–29 kb and temperatures of 1430–1468 °C for their origin. Sen and Chandrasekharam (2011) interpreted an adjusted (Fo_{90} -equilibrated) composition of a Gujarat picrite (PMK) as a primary magma that yielded a mantle potential temperature of ~1550 °C, but noted that PMK could not be parental to the vast majority of the Deccan tholeiites.

Since Sen’s (1995) and Melluso et al.’s (1995) attempts to calculate the composition of primary magmas of the Ambenali tholeiites and Gujarat picrites, many peridotite melting experiments have been performed (e.g., Falloon et al. 1997, 2001; Kinzler 1997; Gaetani and Grove 1998; Robinson et al. 1998; Pickering-Witter and Johnson 2000; Longhi 2002; Wasylenki et al. 2003; Laporte et al. 2004; Till et al. 2012 and references therein). Thermobarometric expressions based on the compositions of the multiple-phase saturated liquids in experiments have been presented by several workers (e.g., Grove et al. 1992; Yang et al. 1996; Herzberg 2004; Villiger et al. 2007; Till et al. 2012). Till et al. (2012) considered a large experimental data set and presented composition-dependent, parameterized expressions to predict the compositions of partial melts and the P–T conditions of multiple saturation points at which the melts are in equilibrium with the phases in plagioclase lherzolite and spinel lherzolite. We use these formulations to constrain the compositions and P–T conditions of equilibration of the primary magmas of an ankaramite-bearing tholeiitic sequence from Mumbai in the western Deccan Traps (Fig. 1a, b). We present petrographic and mineral chemical data on the ankaramite, and based on reverse fractional crystallization (i.e., incremental addition of equilibrium phases) calculations on the ankaramite and the associated tholeiites, we show that their tholeiitic primary magmas last equilibrated with the

mantle at the Moho or with upwelled mantle in the lower crust. We have obtained closely similar results for the parental magmas of the voluminous Ambenali and Mahabaleshwar tholeiites of the Western Ghats sequence.

Geological setting

The Cretaceous–Paleogene Deccan Traps of western India (Fig. 1a) is one of the largest continental flood basalt provinces in the world with a present-day area of $\geq 500,000\text{ km}^2$ (Wadia 1975) on land and a large additional area offshore of western India. The stratigraphy of the Deccan Traps is well established in the Western Ghats escarpment oriented north–south near the western coast of India, where the maximum stratigraphic thickness of the nearly horizontal lava sequence is ~3.4 km (Fig. 1a, Table 1; Cox and Hawkesworth 1985; Beane et al. 1986; Khadri et al. 1988; Subbarao et al. 1988; Lightfoot et al. 1990). The present study area of Mumbai (Fig. 1b) is located west of the escarpment and exposes a regional west-dipping monoclinical structure known as the Panvel flexure related to late-stage extensional tectonics (Sheth 1998; Sheth and Pande 2014; Sheth et al. 2014). The Powai ankaramite, the focus of this study, is located within a tholeiitic lava flow sequence that dips 17–18° toward west-northwest and is cut by numerous tholeiitic dikes in the Ghatkopar–Powai area of the Mumbai city (Fig. 1b; Sheth et al. 2014).

Geochemistry

Bulk-rock geochemical data (major oxides, trace elements, and Nd–Sr isotopic compositions) on the Powai

ankaramite and the associated Ghatkopar–Powai tholeiites are presented in Sheth et al. (2014). Two samples of the ankaramite (MMF6 and MMF7, with 15–12 wt% MgO) and some of the Ghatkopar–Powai tholeiites show trace element and Nd–Sr isotopic compositions [$\epsilon_{\text{Nd}}^t = -3.6$ to -5.5 , $(^{87}\text{Sr}/^{86}\text{Sr})_t = 0.705509\text{--}0.706483$] closely similar to the voluminous Mahabaleshwar Formation in the upper Western Ghats sequence (Table 1), though the geochemical similarities are only partial and no direct stratigraphic correlation is possible (Sheth et al. 2014). The Mahabaleshwar tholeiites have been interpreted as evolved magmas contaminated by low- ϵ_{Nd} , low- $^{87}\text{Sr}/^{86}\text{Sr}$ lithospheric material, either enriched mantle (Lightfoot and Hawkesworth 1988; Lightfoot et al. 1990) or lower crust (Mahoney et al. 1982; Bhattacharya et al. 2013). A few of the Ghatkopar–Powai tholeiites have Nd–Sr isotopic characteristics [$\epsilon_{\text{Nd}}^t = 2.5\text{--}5.6$, $(^{87}\text{Sr}/^{86}\text{Sr})_t = 0.703924\text{--}0.704532$] similar to the voluminous Ambenali Formation lavas underlying the Mahabaleshwar Formation in the Western Ghats (Table 1) and are relatively little contaminated by continental lithosphere.

Analytical methods

Chemical compositions of minerals and groundmass in the Powai ankaramite samples MMF6 and MMF7 were measured on a JEOL JXA-8200 Superprobe electron probe micro-analyzer (EPMA) using an accelerating voltage of 15 kV and a beam current of 10 nA at the Massachusetts Institute of Technology, Cambridge, USA. The raw data were corrected for matrix effects using the CITZAF package (Armstrong 1995). The minerals were analyzed with a beam diameter of 1 μm , counting times of 20–40 s, and the typical 1σ standard deviations from counting statistics were 0.3–1.0 % (for major elements) and 1–5 % (for minor elements) of the analyzed concentrations. The beam diameter was increased to 300 μm to analyze the groundmass in which the average grain size is ~ 100 μm . The standard intensities were calibrated on the Alvin1690-20 mid-oceanic ridge basalt glass (Grove et al. 1992) with a 300- μm beam for the groundmass analysis. The approximate absolute 1σ standard deviations for the replicate analyses of the groundmass are as follows: 2.5 % for SiO_2 , 1 % for TiO_2 , 5 % for Al_2O_3 , 0.1 % for Cr_2O_3 , 3.5 % for FeO, 0.1 % for MnO, 5.5 % for MgO, 3.3 % for CaO, 1 % for Na_2O , 0.4 % for K_2O , 0.15 % for SO_3 , 0.05 % for P_2O_5 , and 0.03 % for NiO. Olivine-hosted melt inclusions and smectitic clay were analyzed with a beam diameter of 10 μm . The calibration was performed on Alvin1690-20 with a 10- μm beam diameter, and the approximate absolute 1σ standard deviations for the replicate analyses of the melt inclusions are as follows: 2.4 % for SiO_2 , 0.4 % for TiO_2 , 0.5 % for

Al_2O_3 , 0.03 % for Cr_2O_3 , 0.5 % for FeO, 0.03 % for MnO, 0.6 % for MgO, 1.5 % for CaO, 0.6 % for Na_2O , 0.2 % for K_2O , 0.05 % for SO_3 , 0.04 % for P_2O_5 , and 0.02 % for NiO. Oxygen was also analyzed in the groundmass and clay, and the H_2O content was calculated by first assigning the available oxygen to form the stoichiometric oxides of the cations and then using the remaining oxygen to form H_2O . The estimated H_2O contents were used to assess low-temperature alteration in the samples.

Back-scattered electron (BSE) images and X-ray elemental maps were also obtained with the same EPMA using a 15 kV voltage and 10 nA beam current. The large-area X-ray maps (4.5 cm \times 2.7 cm) with a resolution of 10 μm were obtained in the stage-rastered mode with a stationary beam to avoid signal loss due to beam and X-ray defocussing associated with beam-rastered images. The area proportions of the phenocrysts and the groundmass were obtained through image analysis using the “ImageJ” software developed at the National Institute of Health, USA. Average proportions of the crystals and the groundmass were calculated by averaging the data obtained from the Mg, Ca, and Al maps, and the BSE image.

Texture and mineral chemistry

In thin section, the Powai ankaramite shows rounded clusters of twinned and radially arranged clinopyroxene up to 5 mm in size, along with smaller olivine crystals, in a fine-grained basaltic groundmass (Fig. 2). In X-ray maps and BSE images, it shows large crystals of augitic clinopyroxene (Aug or Cpx, 3–5 mm in size), olivine (Ol, 1–2 mm in size), and minor plagioclase (Pl, ~ 0.5 mm in size) embedded in a fine groundmass of Ol + Pl + Cpx + Fe oxides (Figs. 3, 4). The abundance of the large augite crystals (22–40 modal %) exceeds that of the large olivine crystals (11–16 modal %, Table 2). Orthopyroxene (Opx, 2–4 mm in size) is minor and is always mantled by a thick overgrowth rim of augite (Fig. 4a). The margins of the orthopyroxene crystals are irregular and embayed. The large augite crystals contain inclusions of olivine and glass (Fig. 4b), and the latter is altered to smectitic clay. The large olivine crystals contain alteration veins and abundant melt inclusions (MI, Fig. 4c), also commonly altered to smectitic clay. The rare unaltered melt inclusions in the olivine cores are 50–100 μm in size, subrounded, and contain “daughter” crystals and occasionally, trapped bubbles (cf. Schiano 2003). The rare plagioclase crystals, much smaller in size than the olivine and augite, have an average composition of $\text{An}_{70}\text{Ab}_{29}\text{Or}_{0.7}$ and also contain olivine inclusions (Fig. 4d).

The large olivine crystals show normal compositional zoning (Fig. 5a). The forsterite content of olivine grain 1 gradually decreases from Fo_{84} to Fo_{80} in the inner ~ 80 %

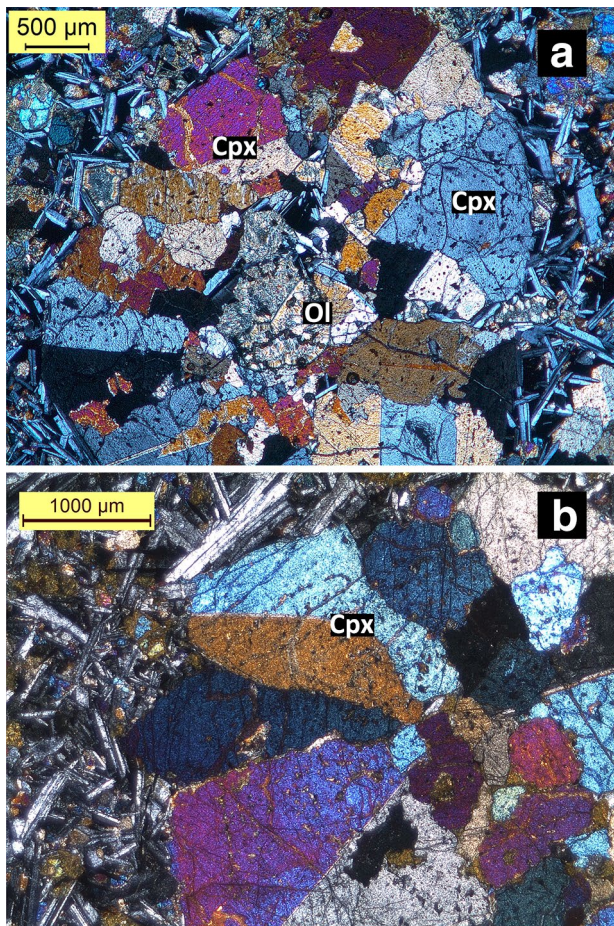


Fig. 2 Thin section photomicrographs of the Powai ankaramite between crossed nicols showing large crystals of olivine (Ol) and sector zoned, twinned and radially arranged clinopyroxene (Cpx) surrounded by a fine-grained groundmass containing plagioclase laths

of the crystal, but drops sharply to Fe_{74} in the outermost rim (Fig. 5a, Table 3). The apparent lower forsterite content of the core of grain 2 compared to the core of grain 1 is probably because the center of the core of grain 2 is not exposed and could not be analyzed. The large augite and orthopyroxene crystals show concentric oscillatory compositional zoning (Fig. 5b,c). Their composition ranges are $En_{59-47}Fs_{10-14}Wo_{27-42}$ for augite and $En_{79-77}Fs_{16-19}Wo_{5-4}$ for orthopyroxene (Fig. 5d), and the average Mg# of both pyroxenes is 82 (Table 3). The Mg# of minor smectitic clay in the groundmass, probably representing altered glass, is ~ 78 (Table 4).

Only a few of the well-preserved melt inclusions not associated with alteration veins within olivine cores could be analyzed. The range of Mg# of these unaltered melt inclusions is 39–45, considering total Fe as Fe^{2+} in the absence of Fe^{3+} data (Table 4). The calculated $K_{D(Fe-Mg)}$ coefficients for Fe^{2+} –Mg distribution between the host olivine core (Fe_{84}) and the melt inclusions show lower values (0.12–0.16,

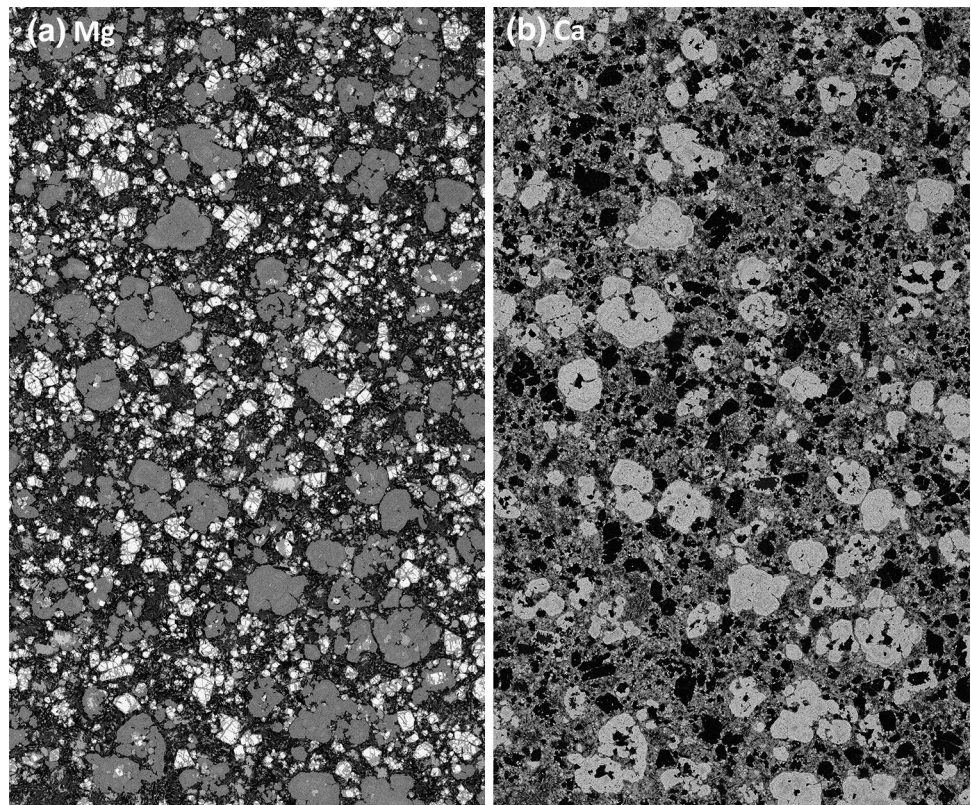
Table 4; or 0.14–0.18, assuming 15 % of the total Fe as Fe^{3+} in melt, cf. Middlemost 1989) than their equilibrium value (0.30 ± 0.03 , Roeder and Emslie 1970). The olivine near the contact with the melt inclusions is relatively Fe rich (Fe_{79} , Table 3) compared to the rest of the olivine core.

The calculated $K_{D(Fe-Mg)}$ values between the large crystals (compositions in Table 3) and the ankaramite bulk rock (compositions from Sheth et al. 2014) are higher (0.39–0.78 for olivine and 0.44–0.54 for pyroxenes; Table 4) than their equilibrium values (0.30 ± 0.03 for olivine, Roeder and Emslie 1970; 0.25 ± 0.02 for clinopyroxene, Grove et al. 1992; 0.275 ± 0.015 for orthopyroxene, Laubier et al. 2010; also see Bédard 2007, 2010 for a compilation and parameterization of Fe–Mg exchange coefficients for Cpx–melt and Opx–melt). Assuming 15 % of the total Fe as Fe^{3+} (cf. Middlemost 1989), the $K_{D(Fe-Mg)}$ values (0.46–0.92 for olivine and 0.52–0.64 for pyroxenes) are even higher. Neither do the large crystals except for the olivine core show equilibrium ($K_{D(Fe-Mg)}$: 0.4–0.5 for olivine and 0.33–0.35 for pyroxenes) with the groundmass that has an Mg# of ~ 61 considering total Fe as Fe^{2+} (Table 4). The Fe_{84} olivine core does show an equilibrium $K_{D(Fe-Mg)}$ with the groundmass, but this may be coincidental because the olivine core was never in contact with the groundmass. Thus, the Powai ankaramite does not represent a liquid but is a cumulate rock containing excess olivine, augite, and orthopyroxene.

Liquid thermobarometry and estimates of primary magma compositions

The majority of Deccan tholeiites represent evolved (differentiated) liquids derived by low-pressure olivine gabbro fractionation from primitive tholeiitic liquids. In Ol–Pl–Cpx and Ol–Cpx–Qz pseudoternary projections of the Ol–Cpx–Qz–Ne basalt tetrahedron (Qz: quartz, Ne: nepheline) (cf. Yoder and Tilley 1962), liquid compositions plot on multiple saturation boundaries (e.g., Ol + Pl, Ol + Pl + Cpx, Ol + Pl + Cpx + Opx) that define the fractional crystallization path of the liquid (Fig. 6). The P–T conditions and the positions of the multiple saturation boundaries for a given bulk composition are calculated with the experimentally constrained equations of Till et al. (2012) and plotted in the basalt tetrahedron using mineral components in terms of their molar monoxides (“oxygen units” of Tormey et al. 1987 and Grove 1993). Estimating composition and P–T of equilibration of the primary magma of a differentiated liquid involves reconstructing its successive parents by moving backward along the low-pressure fractional crystallization paths in small steps (by adding back the crystallized phases), such that the ultimate parental liquid shows equilibrium with peridotite at a higher pressure (Fig. 6). Phases are added in small amounts (1 % of the

Fig. 3 **a** Mg and **b** Ca X-ray elemental maps of ankaramite sample MMF6 showing the distribution of large crystals of olivine and augite in a fine-grained matrix. Olivine appears bright in the Mg map, and augite appears bright in the Ca map. The size of the area mapped is 4.5 cm × 2.7 cm



liquid in each step) and in equilibrium with the changing liquid composition (as constrained by equilibrium values of $K_{D(\text{Fe-Mg})}$ and other elemental distribution coefficients), and their proportions are constrained by the position of the liquid and its multiple saturation boundaries in each step within the tetrahedral space. Commonly, an initial stage of Ol + Pl + Cpx addition is followed by another stage of Ol + Pl addition. During the first stage, the position of the liquid does not change in the Ol–Pl–Cpx diagram, whereas it moves toward the Ol–Cpx sidebar in the Ol–Cpx–Qz diagram. During the second stage, the liquid moves toward the Ol–Pl sidebar in the Ol–Pl–Cpx diagram and toward the Ol apex in the Ol–Cpx–Qz diagram. The proportion of phases, the number of steps in each stage, and the switching point between Ol + Pl + Cpx to Ol + Pl addition are unique so that the final liquid in equilibrium with the mantle phases (e.g., Fo_{89–90} olivine, pyroxene Mg# ~91–92) plots on one of its high-pressure spinel lherzolite multiple saturation points (Fig. 6). Any deviation from these proportions, the number of steps, and the switching point will result in a liquid that may show equilibrium with mantle minerals, but it will not plot on any of its spinel lherzolite multiple saturation points (the liquid may not reach it or go past it) and hence will not qualify as a primary magma. Note that the second stage of Ol + Pl addition may not be required if the liquid already reaches multiple-phase saturation with spinel lherzolite before the switching point.

The success of the above method requires that the differentiated liquid has not been modified by processes other than fractional crystallization of its parent. A composition that does not plot on multiple saturation boundaries represents a liquid that has been modified by processes such as excess crystal accumulation or mixing with a contaminant. In such a case, the liquid composition must be corrected before its parental liquid can be quantified. Here, we use the equations of Till et al. (2012) to calculate the composition and P–T conditions of equilibration of the primary magmas of liquids that are modified only by fractional crystallization and are not significantly contaminated. In addition, the pressure at which evolved liquids (Mg# <60) crystallize in the upper crust is calculated with the equation of Villiger et al. (2007) based on the CaO content and the Mg# of the liquid.

Liquid related to the groundmass of the Powai ankaramite

The measured compositions of the ankaramite groundmass (GM, Table 4) do not plot on any of their respective multiple saturation points in Ol–Pl–Cpx and Ol–Cpx–Qz pseudoternary diagrams (not shown), indicating that they have been modified by a process other than fractional crystallization. Therefore, we first apply corrections to the measured GM compositions to estimate their unmodified compositions as described below.

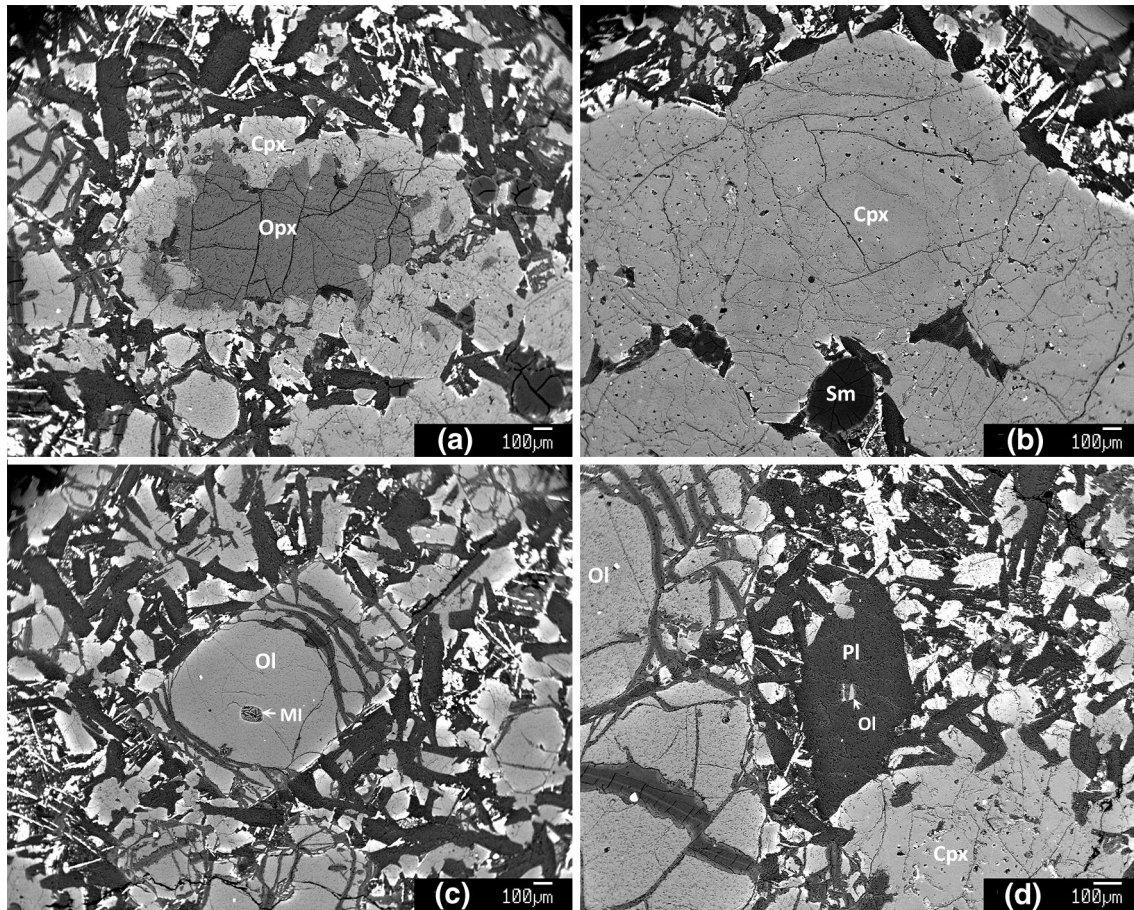


Fig. 4 **a** Augitic clinopyroxene (Cpx) overgrowth on orthopyroxene (Opx). **b** Oscillatory-zoned Cpx with glass inclusion altered to smectitic clay (sm). **c** Olivine (Ol) with alteration veins and melt inclusion

(MI). **d** Plagioclase (Pl) with olivine inclusion. The groundmass is composed of fine-grained Ol + Cpx + Pl + Fe oxides

Table 2 Modal compositions of the Powai ankaramite, Mumbai, Deccan Traps, India

	MMF6		MMF7	
	wt % ^a	1σ	wt % ^a	1σ
Olivine	10.8	0.5	16.3	0.8
Clinopyroxene	30.9	3.7	22.4	4.3
Orthopyroxene	0.6	0.4	0.3	0.0
Plagioclase	0.1	–	0.1	–
Smectitic clay	3.4	0.5	3.5	0.5
Groundmass	54.2	0.8	57.4	1.3

^a Calculated using area % estimates from X-ray and BSE images (considered as vol%), and density (g/cm³) values of 3.3 for olivine, 3.2 for pyroxenes, 2.66 for plagioclase, 2.35 for clay, and 3.0 for groundmass

Orthopyroxene occupies a maximum of ~85 vol% of the combined volume of the Opx + Aug overgrowth (Fig. 4a), and the outer ~15–20 % of the core-to-rim profiles of

olivine show a sharp compositional change (Fig. 5a). In addition, the outer ~15 % of the core-to-rim profile of augite shows a distinct Wo-rich zone (Fig. 5b). This implies that GM formed from a parental liquid GM_{liq} that precipitated the outer ~15 vol% of the olivine and augite, and the augite overgrowth on orthopyroxene. Reconstructing GM_{liq} by combining its crystallization products (15 % of the amounts of olivine and Cpx from Table 2 and using average rim compositions from Table 3) with GM yields a composition with ~50.5 wt% SiO₂ and Mg# 63 (Table 4). However, when we plot the calculated GM_{liq} liquids in Ol–Pl–Cpx and Ol–Cpx–Qz pseudoternary diagrams (Fig. 7), they still do not plot on any of their multiple saturation points predicted with the equations of Till et al. (2012). This is perhaps because GM_{liq} has assimilated orthopyroxene as indicated by the embayed margins of the orthopyroxene crystals (Fig. 4a). We correct for assimilation by subtracting orthopyroxene from GM_{liq} such that the liquid composition moves toward the Pl–Cpx and Ol–Cpx sidebars of the pseudoternary plots and eventually intersects the ~6 kb

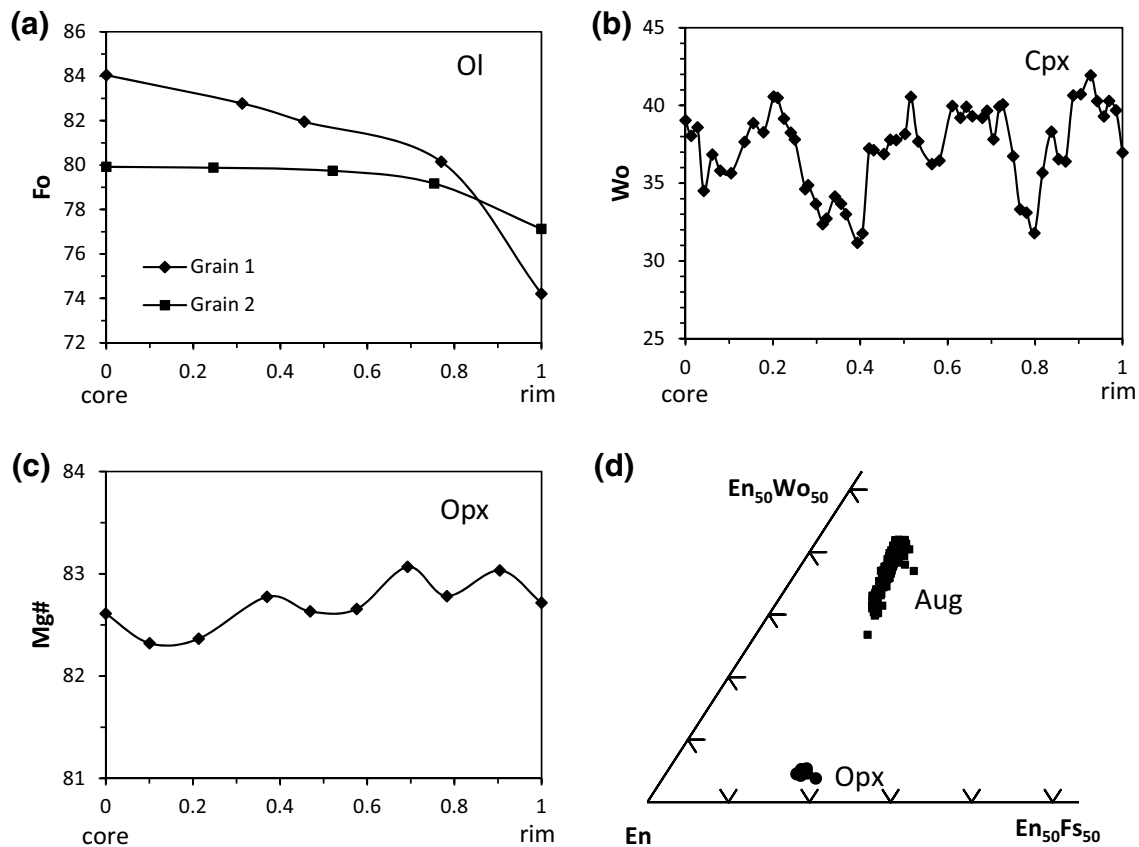


Fig. 5 a–c Core-to-rim variation in the Mg# of olivine, the wollastonite (Wo) content of clinopyroxene, and the Mg# of orthopyroxene. Values on the *x*-axes show fractional distances from the core to the

rim. **d** Pyroxene compositions plotted in the wollastonite–enstatite–ferrosilite (Wo–En–Fs) ternary diagram

Ol + Pl + Cpx saturation point for the corrected liquid (Fig. 7a). The temperature of the corrected liquid $GM_{liq(c)}$ is ~ 1230 °C at 6 kb (Table 5). With Villiger et al.'s (2007) equations, $GM_{liq(c)}$ yields slightly higher equilibration pressures of 6.9 kb (Table 5). The $GM_{liq(c)}$ liquid, resulting from the subtraction of orthopyroxene in an amount equal to 15–17 % of the volume of GM_{liq} , is a tholeiitic liquid with Mg# 53.7 (Table 4) that plots in the basalt field of the total alkali–silica diagram (Fig. 8).

We can now calculate the primary magma composition parental to $GM_{liq(c)}$ by incrementally adding back the phases that must have been fractionated from the successive parental liquids in proportions predicted by the equations of Till et al. (2012). For the $GM_{liq(c)}$ of MMF6, if we use 1 % increments to add equilibrium Ol:Pl:Aug in 16:59:25 proportions as constrained by the Ol + Pl + Cpx saturation point at 6 kb, we obtain a liquid with ~ 49 wt% SiO₂, ~ 10 wt% MgO, and Mg# 73 that is in equilibrium with Fo₉₀ olivine, augite Mg# 92, and orthopyroxene Mg# 91, after 82 steps (Table 5). This liquid, the primary magma of $GM_{liq(c)}$, plots on its predicted spinel lherzolite multiple saturation points at 8–10 kb and 1268–1292 °C (Table 5,

Fig. 7b). The results are very similar to the $GM_{liq(c)}$ of MMF7 (Table 5). Thus, the primary magma of $GM_{liq(c)}$ was in equilibrium with the mantle at 8–10 kb and 1268–1292 °C, and it fractionated 56 % Ol + Pl + Cpx at ~ 6 kb to produce $GM_{liq(c)}$ (82 steps of equilibrium phase addition are equivalent to 56 % fractional crystallization, Table 5).

Melt inclusions within olivine cores in the Powai ankaramite

The measured melt inclusion compositions (MI, Table 4) plot on or near the Pl–Cpx and Cpx–Qz sidebars of the pseudoternary diagrams (Fig. 9). They do not coincide with any of the multiple saturation points predicted with the equations of Till et al. (2012). This can be attributed to modification of the melt composition by post-entrapment olivine crystallization on the inclusion walls with decreasing temperature. Such crystallization is indicated by disequilibrium between the host olivine core (Fo₈₄) and the measured MI ($K_{D(Fe-Mg)}$ 0.12–0.16, Table 4), and the presence of relatively Fe-rich olivine (Fo₇₉, Table 3) near the inclusion-bearing part of the core. Note that the last olivine

Table 3 Compositions of large crystals in the Powai ankaramite, Mumbai, Deccan Traps, India

n	MMF6										MMF7								
	Ol avg	Ol core	Ol rim	Ol rim	Ol near MI	Cpx avg	Cpx rim	Opx avg	Pl avg		Ol avg	Ol rim	Ol rim	Ol near MI	Cpx avg	Cpx rim	Opx avg	Pl avg	
	25	1	2	1	1	94	15	25	10		25	2	1	1	89	15	8	9	
Weight percent																			
SiO ₂	38.87	39.35	38.48	38.62	38.62	53.66	53.29	54.79	51.13		38.80	38.95	38.64	38.64	52.94	52.92	55.14	50.92	
TiO ₂	0.01	0.00	0.05	0.01	0.01	0.49	0.56	0.18			0.02	0.01	0.00	0.00	0.43	0.54	0.21		
Al ₂ O ₃	0.05	0.00	0.26	0.04	0.04	2.45	2.28	1.93	30.92		0.03	0.07	0.02	0.02	2.54	2.58	2.08	30.92	
Cr ₂ O ₃						0.77	0.79	0.47							0.83	0.89	0.55		
FeO	18.91	15.24	22.07	20.18	20.18	7.05	6.91	10.99	0.50		18.99	22.18	19.28	19.28	7.13	6.78	11.25	0.58	
MnO	0.23	0.16	0.26	0.24	0.24	0.19	0.19	0.21			0.24	0.32	0.27	0.18	0.18	0.17	0.22		
MgO	41.84	45.01	38.51	41.24	41.24	18.13	17.39	28.80	0.20		41.97	38.58	41.98	41.98	18.46	17.38	28.93	0.26	
CaO	0.29	0.25	0.34	0.33	0.33	18.34	19.26	2.46	14.36		0.29	0.34	0.31	0.31	17.59	19.28	2.47	14.39	
Na ₂ O						0.23	0.25	0.06	3.24						0.28	0.25	0.02	3.32	
K ₂ O						0.00	0.01	0.00	0.11						0.00	0.00	0.00	0.11	
NiO	0.22	0.34	0.20	0.17	0.17						0.21	0.20	0.20	0.20					
Total	100.44	100.35	100.17	100.81	100.81	101.30	100.94	99.88	100.47		100.55	100.64	100.69	100.69	100.38	100.80	100.87	100.50	
Atomic proportions																			
O	4	4	4	4	4	6	6	6	8		4	4	4	4	6	6	6	8	
Si	0.992	0.989	0.999	0.988	0.988	1.937	1.936	1.947	2.321		0.990	1.006	0.986	0.986	1.928	1.925	1.943	2.314	
Ti	0.000	0.000	0.001	0.000	0.000	0.013	0.015	0.005			0.000	0.000	0.000	0.000	0.012	0.015	0.006		
Al	0.002	0.000	0.008	0.001	0.001	0.104	0.098	0.081	1.654		0.001	0.002	0.001	0.001	0.109	0.111	0.086	1.656	
Cr						0.022	0.023	0.013							0.024	0.026	0.015		
Fe	0.404	0.320	0.479	0.432	0.432	0.213	0.210	0.327	0.019		0.405	0.479	0.411	0.411	0.217	0.206	0.332	0.022	
Mn	0.005	0.003	0.006	0.005	0.005	0.006	0.006	0.006			0.005	0.007	0.006	0.006	0.005	0.005	0.007	0.000	
Mg	1.592	1.686	1.490	1.573	1.573	0.975	0.942	1.526	0.014		1.596	1.485	1.597	1.597	1.002	0.943	1.519	0.017	
Ca	0.008	0.007	0.009	0.009	0.009	0.709	0.750	0.094	0.698		0.008	0.009	0.009	0.009	0.687	0.752	0.093	0.700	
Na						0.016	0.018	0.004	0.285						0.020	0.018	0.001	0.292	
K						0.000	0.001	0.000	0.007						0.000	0.000	0.000	0.007	
Ni	0.005	0.007	0.004	0.003	0.003						0.004	0.004	0.004	0.004					
Sum	3.007	3.011	2.996	3.011	3.011	3.995	3.998	4.003	4.998		3.010	2.993	3.014	3.014	4.004	4.000	4.002	5.008	
Mg#, Ca#	79.8	84.0	75.7	78.5	78.5	82.1	81.8	82.4	71.0		79.8	75.6	79.5	79.5	82.2	82.0	82.1	70.6	
End members																			
En, Fo, An	79.5	83.8	75.3	78.1	78.1	51.4	49.5	78.4	70.5		79.4	75.3	79.2	79.2	52.6	49.6	78.2	70.1	
Fs, Fa, Ab	20.1	15.9	24.2	21.4	21.4	11.2	11.0	16.8	28.8		20.2	24.3	20.4	20.4	11.4	10.9	17.1	29.2	
Wo, La, Or	0.4	0.3	0.5	0.4	0.4	37.4	39.4	4.8	0.7		0.4	0.5	0.4	0.4	36.0	39.5	4.8	0.7	

n: Number of analyses; MI: melt inclusion; Mg#: molar 100 × Mg/(Mg + Fe) for olivine (Ol), clinopyroxene (Cpx) and orthopyroxene (Opx), Fo: forsterite, Fa: fayalite, La: lamite (for Ol), En: enstatite, Fs: ferrosilite, Wo: wollastonite (for Cpx and Opx), Ca# molar 100 × Ca/(Ca + Na), An: anorthite, Ab: albite, Or: orthoclase for plagioclase (Pl)

Table 4 Compositions of bulk rock, melt inclusions, groundmass, and clay in the Powai ankaramite

	MMF6										MMF7											
	Sm avg	Bulk	GM avg	GM _{liq}	GM _{liq(c)}	MI avg	MI _{liq(c)}	Sm avg	Bulk	GM avg	GM _{liq}	GM _{liq(c)}	MI avg	MI _{liq(c)}	Sm avg	Bulk	GM avg	GM _{liq}	GM _{liq(c)}	MI avg	MI _{liq(c)}	
	25	80	80	80	80	4	4	20	80	80	80	80	2	2	20	80	80	80	80	2	2	
Weight percent																						
SiO ₂	51.13	47.80	48.96	50.47	49.75	55.15	52.89	52.04	49.26	49.55	50.66	49.87	53.32	51.71								
TiO ₂	0.02	1.19	1.35	1.33	1.54	2.19	1.88	0.01	1.32	1.43	1.40	1.65	2.21	1.96								
Al ₂ O ₃	4.33	8.76	14.82	14.48	16.71	17.97	15.45	3.78	8.54	14.33	13.97	16.45	16.88	14.96								
Cr ₂ O ₃	0.01		0.04	0.07	0.00	0.02	0.02	0.00		0.04	0.06	0.00	0.06	0.05								
FeO	11.82	11.36	10.54	10.88	10.87	5.56	7.57	12.00	10.95	10.65	11.07	11.06	6.88	8.28								
MnO	0.04	0.18	0.17	0.17	0.17	0.10	0.08	0.03	0.18	0.16	0.16	0.15	0.13	0.11								
MgO	23.54	15.46	9.23	10.34	7.08	1.98	7.45	23.53	12.53	9.44	10.63	6.90	3.16	7.54								
CaO	1.00	9.57	8.45	9.06	10.24	12.67	10.89	0.85	12.35	8.37	8.75	10.06	13.01	11.53								
Na ₂ O	0.09	1.32	2.50	2.43	2.85	3.13	2.69	0.07	1.40	2.54	2.47	2.98	3.18	2.82								
K ₂ O	0.09	0.34	0.53	0.52	0.61	0.84	0.72	0.09	0.30	0.59	0.58	0.69	0.71	0.63								
P ₂ O ₅	0.01	0.12	0.16	0.15	0.18	0.29	0.25	0.00	0.12	0.18	0.18	0.21	0.28	0.24								
SO ₃	0.00		0.05	0.05	0.18	0.10	0.08	0.00		0.05	0.05	0.05	0.16	0.14								
NiO	0.05		0.04	0.04	0.04	0.01	0.01	0.05		0.02	0.02	0.02	0.02	0.01								
H ₂ O	7.98	3.29	3.59					7.75	2.39	3.69												
Total	100.11	99.39	100.42	100.00	100.00	100.00	100.00	100.21	99.34	101.04	100.00	100.04	100.00	100.00								
Mg#	78.0	70.8	60.9	62.9	53.7	38.8	63.7	77.8	67.1	61.2	63.1	52.6	45.0	61.9								
Olivine sample K _{D(Fe-Mg)}																						
Avg		0.61	0.40	0.43	0.29	0.16			0.52	0.40	0.43	0.28	0.21									
Core		0.46	0.30	0.32	0.22	0.12	0.33		0.39	0.30	0.33	0.21	0.16	0.31								
Rim		0.78	0.50	0.54	0.37	0.20			0.66	0.51	0.55	0.36	0.26									
Near MI					0.17																	
Cpx-sample K _{D(Fe-Mg)}																						
Avg		0.53	0.34	0.37	0.25				0.44	0.34	0.37	0.24	0.21									
Rim		0.54	0.35	0.38	0.26				0.45	0.35	0.37	0.24	0.21									
Opx-sample K _{D(Fe-Mg)}																						
Avg		0.52	0.33	0.36	0.25				0.45	0.34	0.37	0.24	0.21									
Pl-sample K _{D(Ca-Ni)}																						
Avg		0.61	1.31	1.19	1.23				0.49	1.32	1.22	1.29										

Bulk data from Sheth et al. (2014), *n*: number of analyses, Mg#: molar $100 \times \text{Mg}(\text{Mg} + \text{Fe})$, assuming all Fe is Fe²⁺, Sm: smectitic clay, MI: melt inclusion, GM: groundmass, subscript liq: liquid, liq(c): corrected liquid, K_D's calculated using compositions in this table and mineral compositions in Table 3; the equilibrium K_D's are italicized, MI_{liq(c)} was calculated by adding 15 % (for MMF6) and 12 % (for MMF7) equilibrium olivine to MI (see text)

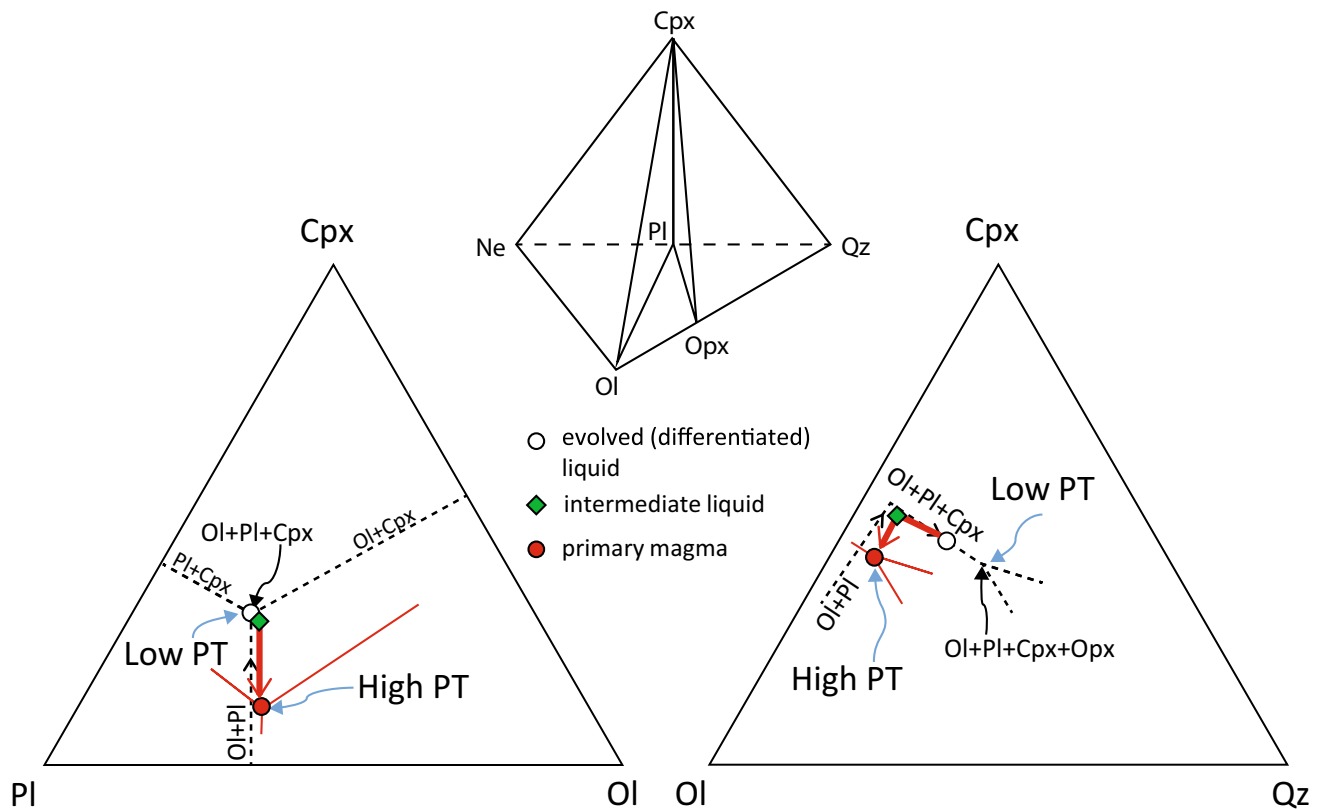


Fig. 6 Ol–Pl–Cpx and Ol–Cpx–Qz pseudoternary projections of the Ol–Cpx–Qz–Ne basalt tetrahedron projected from quartz and plagioclase, respectively. “Low PT” and “high PT” represent low- and high-pressure–temperature invariant points for the Ol + Pl + Cpx + Opx assemblage. A differentiated liquid saturated with Ol + Pl + Cpx plots on its low-pressure fractional crystallization path (dashed lines with black arrows pointing down temperature) that is specific for its composition. Note that the Ol + Pl + Cpx saturation boundary appears as a point in the Ol–Pl–Cpx diagram, and as a line approximately perpendicular to the Ol–Cpx sidebar in the Ol–Cpx–Qz diagram. In addition, the Ol + Pl + Cpx and the Ol + Pl + Cpx + Opx boundaries plot approximately on the same point on the Ol–Pl–Cpx

diagram. The *thick red lines with arrows* trace the liquid backward to its intermediate and primitive parents, and the fractionating assemblage changes from Ol + Pl + Cpx to Ol + Pl at the intermediate liquid composition. Note that the fractional crystallization path shifts with changing liquid compositions, and the *thick red lines with arrows* represent a liquid trajectory with each point on a fractional crystallization path specific to a single liquid composition. If the primitive liquid shows equilibrium with mantle phases (e.g., Fo₉₀ olivine, pyroxene Mg# 91–92) and it plots on one of its high-pressure spinel lherzolite-saturated invariant points (e.g., the “high PT” point), it represents a primary magma in equilibrium with mantle

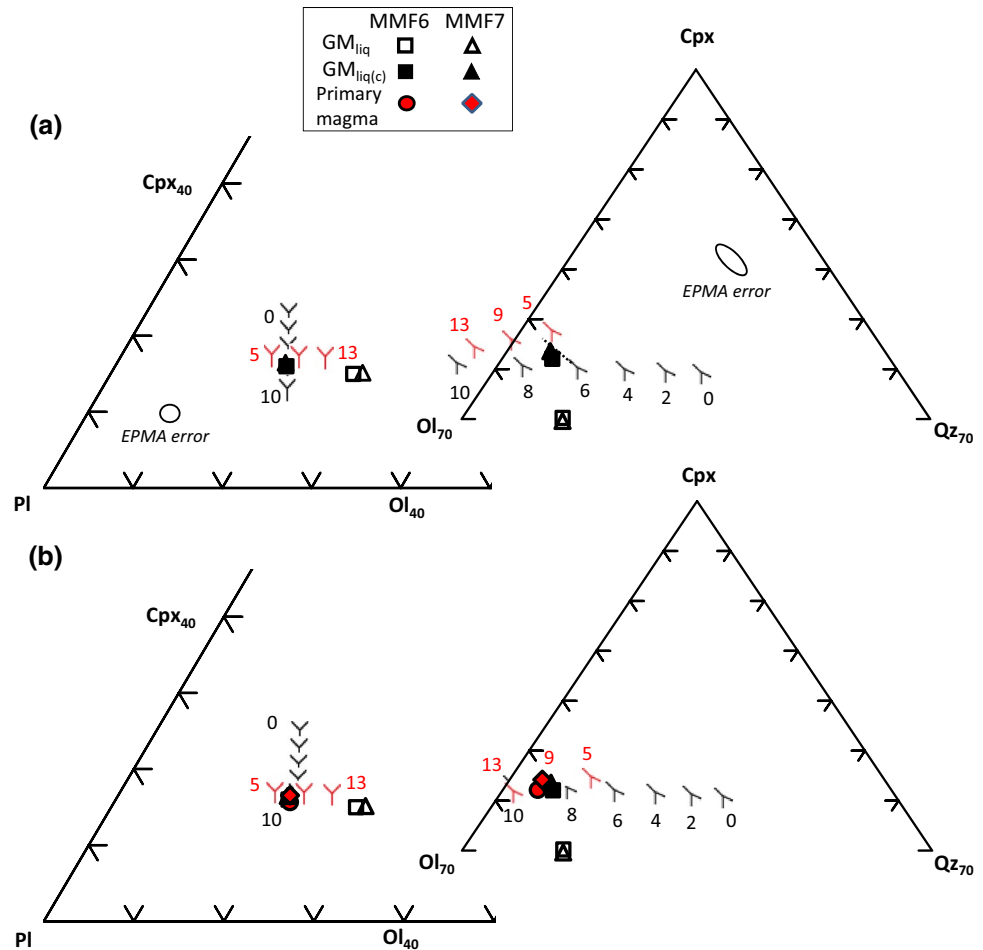
to crystallize in equilibrium with the melt inclusion after entrapment should be even higher in Fe (e.g., Fo₆₈ for the inclusion in MMF6 that has an Mg# of 39) on the innermost wall of the inclusion, and the measured Fo₇₉ composition (Table 3) near the inclusion represents an intermediate olivine crystallized from the melt on the inclusion wall.

To correct for post-entrapment olivine crystallization on the inclusion walls, we add olivine to MI in 1 % increments while maintaining the olivine–melt $K_{D(\text{Fe-Mg})}$ at its equilibrium value of 0.30 (cf. Roeder and Emslie 1970). The resulting melt compositions move toward the olivine apex and eventually intersect one of their low-pressure Ol + Pl + Cpx saturation points predicted by the equations of Till et al. (2012). For sample MMF6, 15 % equilibrium olivine addition resulted in a liquid (MI_{liq(c)}) saturated with Ol (Fo₈₅) + Pl + Cpx at 2 kb. For MMF7, 12 % equilibrium olivine was added to generate

MI_{liq(c)} saturated with Ol (Fo₈₄) + Pl + Cpx at 1 bar. The temperatures of the MI_{liq(c)} liquids were ~1190–1210 °C (Table 5). The Fo_{84–85} olivine in equilibrium with MI_{liq(c)} is similar to the composition of the olivine core (Fo₈₄) in the ankaramite, and the calculated $K_{D(\text{Fe-Mg})}$ values (0.31–0.33, Table 4) for the olivine core–MI_{liq(c)} pair are close to the equilibrium value. The MI_{liq(c)} liquids are tholeiitic with 52–53 wt% SiO₂ and Mg# 62–64 (Table 4), and they plot in the basalt and basaltic andesite fields of the total alkali–silica diagram (Fig. 8).

To calculate the composition of the primary magma of MI_{liq(c)} in MMF6, we initially added equilibrium Ol:Pl:Aug in 14:61:25 proportions and then equilibrium Ol:Pl in 28:72 proportions to MI_{liq(c)}, as predicted by its multiple saturation boundaries at 2 kb, in 1 % increments. After 16 steps in the initial stage and an additional 14 steps in the second stage, we obtained a liquid with ~52 wt% SiO₂, 8.7 wt% MgO, and

Fig. 7 Ol–Pl–Cpx pseudoternary diagrams projected from quartz and Ol–Cpx–Qz pseudoternary diagrams projected from plagioclase with the groundmass-related liquids in the Powai ankaramite plotted in oxygen units (after Tormey et al. 1987 and Grove 1993). The multiple-phase lherzolite saturation boundaries are calculated with the expressions of Till et al. (2012) at different pressures (black: 0.001–10 kb in 2-kb interval for plagioclase lherzolite, 0 depicts 1 bar; red: 5–13 kb in 4-kb interval for spinel lherzolite) for the liquid in sample MMF6: **a** $GM_{liq(c)}$ and **b** primary magma of $GM_{liq(c)}$. The multiple saturation boundaries for the groundmass-related liquid in MMF7 are at similar positions (not shown for clarity). Note that in **(a)** the $GM_{liq(c)}$ liquids plot on the Ol + Pl + Cpx point at 6 kb in the left panel and the Ol + Pl + Cpx line at 6 kb (dotted line) in the right panel. The error ellipses shown for EPMA analysis are applicable to all pseudoternary diagrams in this article



Mg# 71 that is in equilibrium with Fo_{89} olivine, augite Mg# 91, and orthopyroxene Mg# 90 (Table 5). This liquid, the primary magma of $MI_{liq(c)}$, plots on its predicted spinel lherzolite multiple saturation points at 5–8 kb and 1227–1283 °C (Fig. 9a), and it fractionated 13 % Ol + Pl and another 13 % Ol + Pl + Cpx at 2 kb to generate the $MI_{liq(c)}$ in MMF6 (Table 5).

To calculate the composition of the primary magma of $MI_{liq(c)}$ in MMF7, we added equilibrium Ol:Pl in 3:7 proportions to $MI_{liq(c)}$, as predicted by its multiple saturation point at 1 bar, in 1 % increments. After 38 steps, the liquid with ~50 wt% SiO_2 , 9.6 wt% MgO, and Mg# 71.5 was in equilibrium with Fo_{89} olivine, augite Mg# 92, and orthopyroxene Mg# 90 (Table 5). This primary magma plots on its spinel lherzolite multiple saturation point at 9 kb and 1276 °C (Fig. 9b), and it fractionated 32 % Ol + Pl to generate the $MI_{liq(c)}$ in MMF7 (Table 5).

The pressure range for the primary magmas of the melt inclusions (5–9 kb) overlaps with that for the primary magmas of the groundmass-related liquids (8–10 kb) in the Powai ankaramite. However, the results for the melt inclusions are based on only a few analyses, and the lower pressure estimates (i.e., ~5 kb) require verification with further investigation.

The Ghatkopar–Powai tholeiites

The bulk compositions of the Ghatkopar–Powai tholeiitic flows and dikes plot in the basalt and basaltic andesite fields of the total alkali–silica diagram (Fig. 8). The flows and dikes with a Mahabaleshwar-type trace element and isotopic signature (indicating contamination with enriched mantle or lower crust, Sheth et al. 2014) show a large scatter in pseudoternary plots (not shown), indicating that their compositions have been modified by processes such as crystal accumulation and contamination (refer to Table 1 for the location of the formations in the Deccan stratigraphy). On the other hand, the aphyric dikes with an Ambenali-type isotopic signature (indicating low levels of contamination), some dikes with convex-downward rare earth element patterns (unique among Deccan tholeiites, designated as “CREEP dikes” by Sheth et al. 2014), and two Mahabaleshwar-type dikes, MMD3 and MMD9, are tightly clustered in the Ol–Pl–Cpx pseudoternary plot and show a silica enrichment trend in the Ol–Cpx–Qz pseudoternary plot (Fig. 10a). Importantly, each of these samples plots close to its 1 bar Ol + Pl + Cpx saturation point, indicating that they represent liquids with temperatures of ~1160–1220 °C

Table 5 Calculated compositions of the Deccan primary magmas and their P–T conditions of equilibration

	SiO ₂	TiO ₂	Al ₂ O ₃	Cr ₂ O ₃	FeO	MnO	MgO	CaO	Na ₂ O	K ₂ O	P ₂ O ₅	Mg# ^c			
												bulk	Ol	Cpx	Opx
MMF6 GM _{liq(c)}	49.75	1.54	16.71	0.00	10.87	0.17	7.08	10.24	2.85	0.61	0.18	53.7	79.5	83.5	81.1
	49.23	0.78	18.68	0.00	6.61	0.00	10.02	12.08	2.26	0.27	0.08	73.0	90.0	92.2	90.9
MMF7 GM _{liq(c)}	49.87	1.65	16.45	0.00	11.06	0.15	6.90	10.06	2.98	0.69	0.21	52.6	78.8	82.9	80.5
	49.40	0.82	18.42	0.00	6.60	0.00	9.94	12.11	2.32	0.30	0.09	72.9	90.0	92.1	90.9
MMF6 MI _{liq(c)}	52.89	1.88	15.45	0.02	7.57	0.08	7.45	10.89	2.69	0.72	0.25	63.7	85.4	88.4	86.7
	52.47	1.64	16.15	0.00	6.89	0.00	8.03	11.42	2.58	0.62	0.21	67.5	87.4	90.0	88.5
	51.75	1.43	17.09	0.00	6.41	0.00	8.74	11.37	2.51	0.54	0.18	70.8	89.0	91.4	90.0
MMF7 MI _{liq(c)}	51.71	1.96	14.96	0.05	8.28	0.11	7.54	11.53	2.82	0.63	0.24	61.9	84.4	87.6	85.7
	50.25	1.35	17.44	0.00	6.86	0.00	9.64	11.29	2.57	0.43	0.17	71.5	89.3	91.6	90.3
MMD3 ^a	50.91	2.35	14.57	0.00	12.58	0.20	5.64	10.76	2.21	0.52	0.25	44.4	72.7	77.7	74.8
	49.67	1.26	16.96	0.00	8.41	0.00	8.76	12.76	1.82	0.26	0.12	65.0	86.1	89.0	87.3
	48.93	1.02	18.17	0.00	7.51	0.00	9.78	12.51	1.77	0.21	0.10	69.9	88.6	91.0	89.6
MMD9 ^a	54.54	2.01	13.00	0.00	13.60	0.21	4.47	8.51	2.30	1.10	0.26	36.9	66.1	71.8	68.4
	50.49	0.84	16.74	0.00	7.88	0.00	9.69	12.13	1.77	0.39	0.09	68.7	88.0	90.5	89.0
	50.03	0.75	17.41	0.00	7.41	0.00	10.18	12.04	1.76	0.35	0.08	71.0	89.1	91.4	90.1
MMD6 ^a	51.48	2.45	13.35	0.00	13.52	0.20	5.95	10.28	2.26	0.29	0.22	43.9	72.3	77.3	74.4
	49.93	1.18	16.07	0.00	8.36	0.00	9.80	12.63	1.82	0.12	0.10	67.6	87.5	90.1	88.6
	49.17	0.97	17.30	0.00	7.48	0.00	10.76	12.37	1.78	0.10	0.08	71.9	89.5	91.8	90.5
MMD12 ^{a,d}	48.01	2.65	13.63	0.00	15.37	0.22	6.27	11.43	2.12	0.01	0.29	42.1	70.8	76.0	72.9
	47.53	2.03	15.77	0.00	13.51	0.00	7.58	11.29	2.06	0.01	0.22	50.0	76.9	81.3	78.7
	48.02	0.91	17.62	0.00	7.51	0.00	11.31	12.88	1.66	0.00	0.09	72.9	90.0	92.1	90.9
MMD13 ^a	50.59	2.88	13.17	0.00	14.05	0.22	5.92	10.68	2.21	0.03	0.26	42.9	71.5	76.6	73.6
	49.71	1.45	15.66	0.00	9.02	0.00	9.42	12.77	1.83	0.01	0.12	65.0	86.1	89.0	87.3
	48.80	1.11	17.46	0.00	7.74	0.00	10.56	12.44	1.78	0.01	0.09	70.9	89.0	91.4	90.0
MMD14 ^a	50.25	2.46	13.06	0.00	14.46	0.22	6.22	10.36	2.69	0.05	0.22	43.4	71.9	76.9	74.0
	50.11	1.86	14.21	0.00	12.13	0.00	7.68	11.33	2.48	0.04	0.16	53.0	79.0	83.1	80.7
	49.50	1.54	15.65	0.00	10.98	0.00	8.56	11.19	2.41	0.03	0.14	58.1	82.2	85.8	83.7
	49.24	0.91	16.97	0.00	7.36	0.00	11.12	12.27	2.06	0.02	0.07	72.9	90.0	92.1	90.9
MMD1 ^a	52.37	0.92	13.42	0.00	13.01	0.22	6.45	10.74	2.01	0.70	0.16	46.9	74.6	79.3	76.6
	50.84	0.63	14.97	0.00	9.46	0.00	9.45	12.44	1.73	0.39	0.09	64.0	85.6	88.6	86.8
	49.39	0.46	17.30	0.00	7.88	0.00	10.75	12.21	1.66	0.28	0.06	70.9	89.0	91.4	90.0
MMD7 ^a	52.34	0.87	13.50	0.00	12.17	0.20	7.13	11.52	1.78	0.34	0.14	51.1	77.7	82.0	79.5
	50.75	0.59	14.98	0.00	8.66	0.00	10.24	12.98	1.55	0.18	0.08	67.8	87.5	90.2	88.6
	49.39	0.45	16.76	0.00	7.43	0.00	11.77	12.51	1.49	0.14	0.06	73.8	90.4	92.5	91.3
MMD10 ^a	52.34	0.87	13.50	0.00	12.17	0.20	7.13	11.52	1.78	0.34	0.14	51.1	77.7	82.0	79.5
	50.75	0.59	15.11	0.00	8.64	0.00	10.10	12.99	1.56	0.19	0.08	67.6	87.4	90.1	88.5
	49.49	0.45	17.12	0.00	7.38	0.00	11.14	12.70	1.52	0.14	0.06	72.9	90.0	92.1	90.9
MMD11 ^a	52.46	0.82	13.57	0.00	11.68	0.21	7.27	11.19	2.12	0.56	0.12	52.6	78.7	82.8	80.4
	51.35	0.63	14.60	0.00	9.20	0.00	9.55	12.35	1.88	0.37	0.08	64.9	86.1	88.9	87.3
	49.80	0.45	17.05	0.00	7.61	0.00	10.89	12.08	1.80	0.26	0.06	71.8	89.5	91.7	90.4
Khopoli ^b	51.62	1.12	13.89	0.00	12.04	0.20	7.27	10.55	2.17	0.72	0.00	51.8	78.2	82.4	79.9
	50.80	0.80	15.20	0.00	9.30	0.00	9.50	12.03	1.91	0.46	0.00	64.6	85.9	88.8	87.1
	49.53	0.60	17.26	0.00	7.88	0.00	10.69	11.89	1.82	0.34	0.00	70.8	89.0	91.3	90.0
Ambenali ^c	49.07	2.62	14.11	0.00	13.59	0.23	6.46	10.84	2.57	0.24	0.26	45.9	73.9	78.7	75.8
	49.04	1.33	16.25	0.00	8.60	0.00	9.70	12.82	2.02	0.11	0.12	66.8	87.0	89.7	88.2
	48.23	0.99	18.07	0.00	7.24	0.00	10.94	12.44	1.91	0.08	0.09	72.9	90.0	92.1	90.9

Table 5 continued

	SiO ₂	TiO ₂	Al ₂ O ₃	Cr ₂ O ₃	FeO	MnO	MgO	CaO	Na ₂ O	K ₂ O	P ₂ O ₅	Mg# ^c			
												bulk	Ol	Cpx	Opx
Mahabaleshwar ^c	50.14	2.37	14.31	0.00	12.26	0.18	6.96	10.59	2.54	0.41	0.23	50.3	77.1	81.5	78.9
	49.67	1.39	16.03	0.00	8.51	0.00	9.58	12.38	2.10	0.22	0.13	66.7	87.0	89.7	88.1
	48.97	1.12	17.43	0.00	7.52	0.00	10.52	12.15	2.02	0.18	0.10	71.4	89.3	91.6	90.2
	P (kb) ^f	T (°C) ^f	P (kb) ^h	prop. ⁱ			Steps ⁱ 1 %		F ⁱ %		P (kb) ^j	T (°C) ^j			
				Ol	Pl	Aug									
MMF6	6	1232	6.9												
GM _{liq(c)}				16	59	25	82	56				8–10	1268–1292		
MMF7	6	1231	6.9												
GM _{liq(c)}				15	58	27	85	57				8–10	1268–1292		
MMF6 MI _{liq(c)}	2	1208													
	2	1209		14	61	25	16	13							
				28	72		14	13				5–8	1227–1283		
MMF7 MI _{liq(c)}	0.001	1190		30	70		38	32				9	1276		
MMD3 ^a	0.001	1192	−0.5												
	2	1214		15	56	29	71	41							
				30	70		21	19				6–9	1245–1281		
MMD9 ^a	0.001	1161	3.8												
	6	1246		18	55	28	105	58							
				30	70		11	10				8	1268		
MMD6 ^a	0.001	1195	1.0												
	2	1216		16	53	31	86	47							
				31	69		20	18				9	1284		
MMD12 ^{a,d}	0.001	1207	−4.4												
	6 ^g	1261 ^g		31	69		27	9							
				17	53	30	95	62				9–11	1287–1311		
MMD13 ^a	0.001	1210	−1.1												
	2	1222		15	52	33	78	41							
				30	70		27	24				8–10	1272–1296		
MMD14 ^a	0.001	1193	0.4												
	0.001	1191		15	52	33	32	12							
	6 ^g	1250 ^g		30	70		19	9							
				17	53	30	65	48				9–10	1284–1296		
MMD1 ^a	0.001	1159	1.0												
	2	1197		16	49	35	58	32							
				30	70		32	28				9	1280		
MMD7 ^a	0.001	1171	0.4												
	0.001	1184		17	50	37	58	33							
				34	66		28	25				9–11	1285–1309		
MMD10 ^a	0.001	1171	0.4												
	2	1204		16	51	33	60	19							
				30	70		87	58				9	1284		
MMD11 ^a	0.001	1163	2.6												
	0.001	1175		16	48	36	43	25							
				30	70		33	28				8–10	1268–1292		

Table 5 continued

	P (kb) ^f	T (°C) ^f	P (kb) ^h	prop. ⁱ			Steps ⁱ 1 %	F ⁱ %	P (kb) ^j	T (°C) ^j
				Ol	Pl	Aug				
Khopoli ^b	0.001	1165	4.6							
	0.001	1177		16	51	34	46	28		
				30	70		29	25	10	1290
Ambenali ^c	0.001	1199	0.0							
	2	1217		15	53	32	78	40		
				30	70		30	26	8–13	1272–1332
Mahabaleshwar ^c	0.001	1194	3.5							
	2	1215		15	53	32	62	37		
				30	70		22	20	9–10	1282–1294

Liquid compositions (weight percent; primary magma in bold font) on anhydrous basis. All calculations are based on the equations of Till et al. (2012) except as noted below. The initial compositions are from this study (MMF6 and MMF7)

^a Sheth et al. (2014), ^b Cucciniello et al. (2014), and ^c averages from Beane et al. (1986) and Lightfoot et al. (1990), ^d lowest SiO₂ sample, ^e mineral Mg#s calculated using mineral–melt $K_{D(Fe-Mg)}$'s of 0.30 for Ol, 0.23 for Cpx, and 0.27 for Opx, ^f P–T for initial and intermediate liquids saturated with Ol + Pl + Aug (except ^g P–T for liquids saturated with Ol + Pl + Aug + Opx), ^h crystallization pressures of liquids with Mg# <60 using Villiger et al. (2007) equation, ⁱ proportion of phases added to liquid in previous row in steps of 1 % of the remaining liquid to generate the liquid composition on left (F: %fractional crystallization required to generate liquid in previous row given by the formula $100 \times (1-0.99^n)$, where n is the number of steps), ^j P–T conditions of equilibration of the primary magma with spinel lherzolite

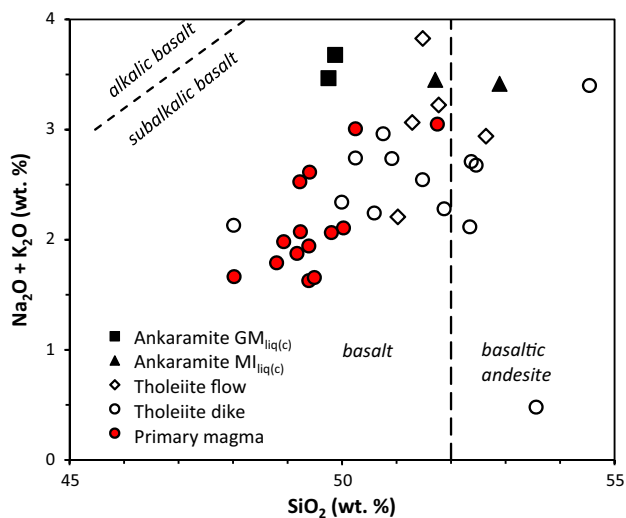


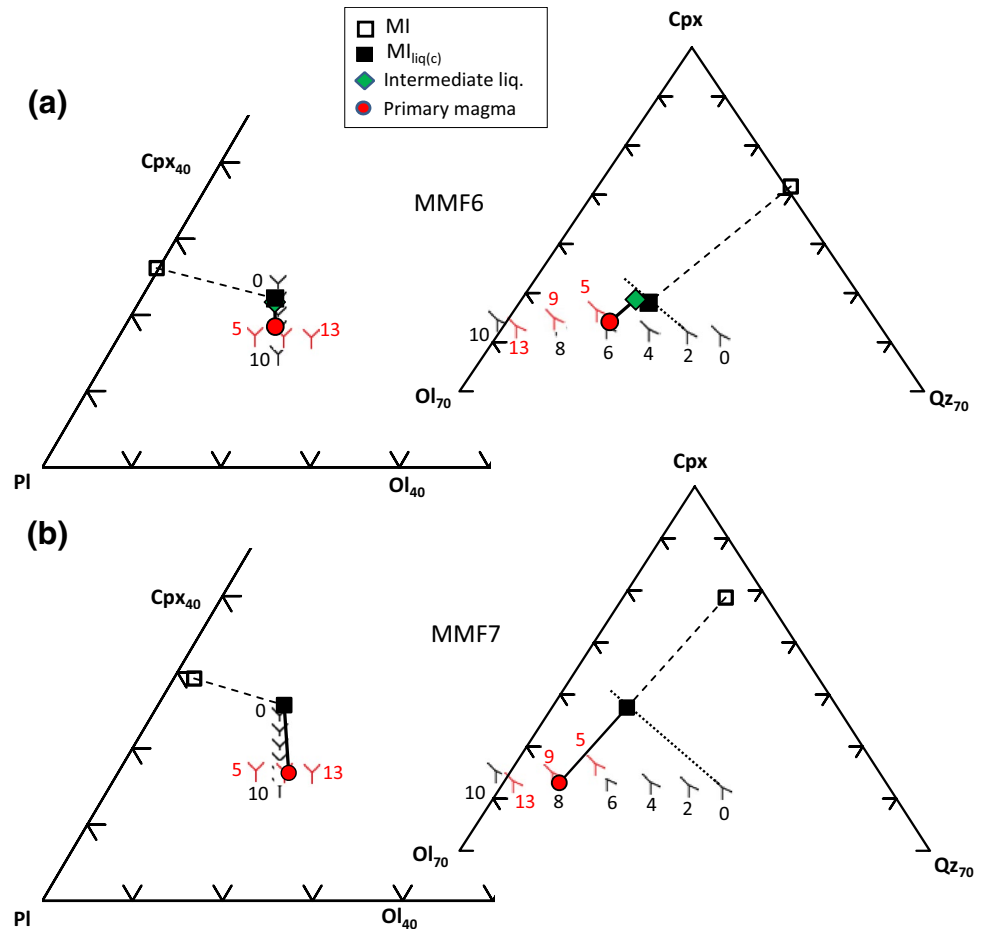
Fig. 8 Total alkali–silica plot (after Le Bas et al. 1986) showing the corrected compositions of the liquids related to the groundmass ($GM_{liq(c)}$) and the olivine-hosted melt inclusions ($MI_{liq(c)}$) in the Powai ankaramite, the bulk compositions of Ghatkopar–Powai tholeiitic flows and dikes (Sheth et al. 2014), and the calculated primary magma compositions (Table 5) for the aphyric tholeiites and the liquids in ankaramite. The alkali basalt–subalkalic basalt (tholeiite) boundary is from Macdonald and Katsura (1964)

(Table 5) that have undergone various degrees of shallow-level Ol + Pl + Cpx fractionation manifested in the silica enrichment trend in the Ol–Cpx–Qz plot (Fig. 10a). With Villiger et al.'s (2007) equation, these liquids yield crystallization pressures <3.8 kb (Table 5). We calculated the primary magmas of these liquids using the same procedure that we used for

the liquids in the ankaramite. For all of these samples except the lowest SiO₂ one, equilibrium Ol + Pl + Cpx was added first, followed by equilibrium Ol + Pl addition. The lowest SiO₂ sample (MMD12) required only Ol + Pl addition. Addition of Ol + Pl + Cpx moved the liquid compositions toward the Ol–Cpx sideline along the silica enrichment trend in the Ol–Cpx–Qz plot until they reached the lowest SiO₂ sample of the trend. From this point, Ol + Pl were added to the liquid until it intersected one of the high-pressure spinel lherzolite multiple saturation points. Except for two samples (MMD12 and MMD14), all of the reconstructed liquids with 49–50 wt% SiO₂, 9.8–11.8 wt% MgO, and Mg# 70–74 are in equilibrium with Fo_{89–90} olivine, augite Mg# 91–92, and orthopyroxene Mg# 90–91 (Table 5), and plot, with one exception, on their respective spinel lherzolite multiple saturation points at ~8–11 kb and ~1268–1309 °C (Fig. 10b). Thus, these are the primary magmas of the uncontaminated Ghatkopar–Powai tholeiites. The exception is the primary magma of MMD3 that seems to have equilibrated at P–T values as low as 6 kb and 1245 °C. Although this result is similar to the lower P–T result for the melt inclusions in MMF6 (5 kb, 1227 °C), such low pressures (5–6 kb) of equilibration for primary magmas are suspect until verified with further work.

The parental magmas of the Ambenali-type dikes MMD12 and MMD14 show equilibrium with Ol + Pl + Cpx + Opx at ~6 kb and ~1250–1261 °C (Table 5). However, these parental magmas with Mg# 50–58 are in equilibrium with Fo_{77–82} olivine, augite Mg# 81–86, and orthopyroxene Mg# 79–84 (Table 5). Thus, they are not primary magmas. But interestingly, they are similar in composition to the groundmass-related liquids

Fig. 9 Ol–Pl–Cpx and Ol–Cpx–Qz pseudoternary diagrams with liquids related to the olivine-hosted melt inclusions in the Powai ankaramite plotted as in Fig. 7. The multiple-phase lherzolite saturation boundaries are for the primary magmas of the melt inclusions in samples (a) MMF6 and (b) MMF7. The crystallization assemblage changes from Ol + Pl to Ol + Pl + Cpx at the intermediate liquid composition for MMF6. The *dashed lines* connect the analyzed compositions MI, with the Fo_{84-85} -corrected compositions $MI_{liq(c)}$, and the *solid lines* represent the fractionation (or mineral addition) paths. The Ol + Pl + Cpx saturation boundary plots as a point in the *left panels* and as a line (*dotted line*) in the *right panels*. The $MI_{liq(c)}$ liquids plot on the Ol + Pl + Cpx saturation boundary at 2 kb in (a) and at 1 bar in (b). Note that in (b), Ol + Pl + Cpx addition was not required to calculate the primary magma



$GM_{liq(c)}$ of the Powai ankaramite (Mg# 53–54, Table 5) that also show equilibrium pressures of ~6 kb and temperatures of ~1230 °C (Table 5). Villiger et al.'s (2007) equation yields a crystallization pressure of 5.7 kb for the parental magma of MMD14. Reverse fractional crystallization of Ol + Pl + Cpx constrained by the 6-kb multiple saturation points of the parental magmas of MMD12 and MMD14 yields spinel lherzolite-equilibrated primary magmas at 9–11 kb and 1284–1311 °C (Table 5). Remarkably, the evolved parental liquid (Mg# 52) of the Khopoli olivine gabbro cumulate intrusion outcropping at the foot of the Western Ghats escarpment east of Mumbai (Fig. 1b, Cucciniello et al. 2014) also yields a primary magma that equilibrated with spinel lherzolite at ~10 kb and ~1290 °C and that has a composition similar to the primary magmas of the Ghatkopar–Powai tholeiites (Fig. 10, Table 5).

Degree of mantle melting

The degree of partial melting of the mantle to generate the primary magmas of the Ghatkopar–Powai tholeiites was

estimated by comparing the incompatible trace element contents of the calculated primary magmas with those of the calculated partial melts of the mantle under the Deccan Traps. Mantle xenoliths are very rare in the Deccan rocks, but the sub-Deccan mantle composition was inferred from the ultramafic xenoliths within the alkali basalts and basanites of Kachchh (Kutch) in the northwestern part of the Deccan province (Fig. 1a). The average trace element contents of the Kachchh mantle (KM) were calculated using the mineral compositions and modes of the spinel lherzolite xenoliths B1, B9, D1, D9, and DD9 (Karmalkar et al. 2000) (Table 6). The trace element contents of partial melts of KM were modeled (Fig. 11) with the non-modal batch melting equation (Shaw 1970) using melting modes for spinel lherzolite (Kinzler and Grove 1992) and average mineral–melt partition coefficients (K_d , Table 6, GERM 2014). These trace element concentrations were compared with the reconstructed trace element concentrations in the primary magmas of the least contaminated, Ambenali-type Ghatkopar–Powai tholeiites (dike samples MMD6, MMD12, MMD13, and MMD14, Sheth et al. 2014) by adding equilibrium phases in the same proportions and number of steps as for the major elements (Table 5), and

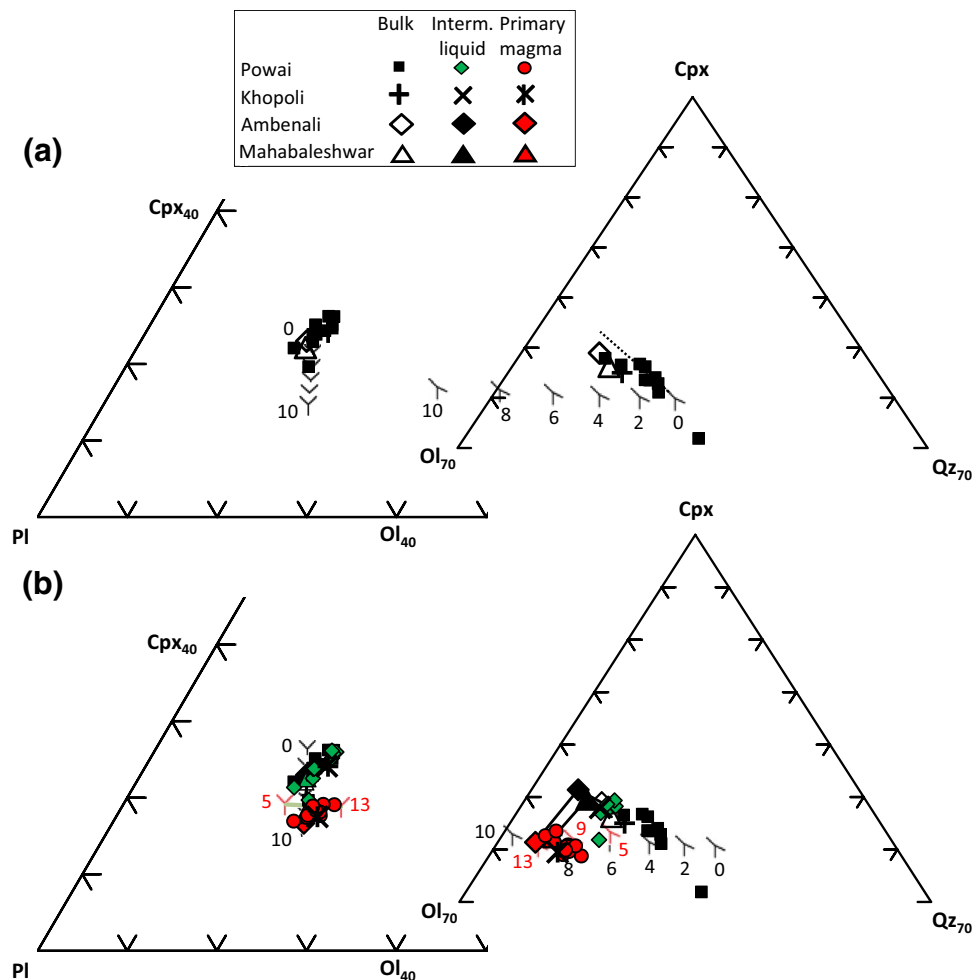


Fig. 10 OI-Pl-Cpx and OI-Cpx-Qz pseudoternary diagrams with Deccan tholeiites and their primary magmas plotted as in Fig. 7. The multiple-phase lherzolite saturation boundaries are for **a** Ghatkopar-Powai tholeiitic dike MMD13 and **b** its primary magma. The multiple saturation boundaries for the other tholeiites are similar to those of MMD13 but not shown for clarity. The bulk compositions of the Ghatkopar-Powai tholeiites are from Sheth et al. (2014), the parental liquid composition of the Khopoli gabbro is from Cucciniello et al. (2014), and the average Ambenali and Mahabaleshwar tholeiite com-

positions are from Beane et al. (1986) and Lightfoot et al. (1990). The crystallization assemblage changes from OI + Pl to OI + Pl + Cpx at the intermediate liquid compositions. The dotted line in the right panel of **a** represents the OI + Pl + Cpx boundary at 1 bar for MMD13. The lines connecting the Ambenali symbols (diamonds) and the lines connecting the Mahabaleshwar symbols (triangles) represent the fractionation paths of the Ambenali and Mahabaleshwar primary magmas

using average K_d values (Table 6, GERM 2014). Rayleigh fractionation calculations starting from the primary magma compositions and subtracting mineral phases in proportions and up to the percentages of fractional crystallization given in Table 5 closely reproduce the evolved Ambenali-type Ghatkopar-Powai tholeiite compositions. The Zr-Nb, Ce-Y, and Th-Ce systematics indicate ~3–5, ~6–10, and ~7–15 % batch partial melting of the Kachchh spinel lherzolites to produce the Ghatkopar-Powai primary magmas (Fig. 11). We conclude that the mantle under the Deccan may have undergone ≤ 15 % batch melting to generate the Ambenali-type primary magmas in the Ghatkopar-Powai area.

Discussion

Possible origin of the Powai ankaramite

As mentioned above, orthopyroxene exclusively occurs within augite overgrowths in the Powai ankaramite. What might have been the origin of the orthopyroxene? It has an Mg# of 82 (Table 3) implying that it crystallized from an evolved basaltic magma and cannot represent mantle orthopyroxene (which has an Mg# of ~91, e.g., Morgan et al. 2008). Assimilation of upper continental crust can make the parental magma Si rich such that it crystallizes orthopyroxene, as found in some Deccan dikes in the Tapi

Table 6 Partition coefficients, mineral modes, and trace element contents used to estimate degree of mantle melting

	Zr	Nb	Th	Ce	Y	Avg. mode in Kachchh xenoliths ^a wt. fraction	Melting proportion ^b wt. fraction
Mineral–melt partition coefficients, K_d^c							
Olivine	0.02	0.00	0.01	0.00	0.03	0.60	−0.30
Plagioclase	0.01	0.03	0.15	0.12	0.03		
Clinopyroxene	0.26	0.01	0.00	0.09	0.41	0.07	0.82
Orthopyroxene	0.02	0.03	0.00	0.00	0.20	0.19	0.40
Spinel	0.02	0.01	0.00	0.00	0.00	0.13	0.08
Concentration in Kachchh xenoliths ^a (ppm)							
B1	1.12	0.16	0.12	0.50	0.96		
B9	2.46	0.15	0.01	0.58	0.88		
D1	6.69	0.35	0.06	2.02	2.00		
D9	1.75	0.09	0.01	0.39	0.60		
DD9	1.74	0.13	0.01	0.48	0.61		
Average	2.75	0.18	0.04	0.79	1.01		
Concentration in Ambenali-type dikes ^d (ppm)							
MMD6	153	13	1.45	29.9	31.5		
MMD12	147	9.8	1.04	26.1	32.7		
MMD13	171	11	1.21	27.3	37.3		
MMD14	125	8.3	0.9	21.4	27.3		

Non-modal batch melting equation (Shaw 1970): $C_i/C_0 = 1/[D_0 + F(1 - P)]$, where C_i , C_0 : concentrations of the trace element in melt and source rock, D_0 : bulk K_d , P : K_d for bulk composition of melting mode, F : fraction of melt. Rayleigh fractionation equation: $C_m/C_{m(0)} = F^{(D-1)}$, where C_m , $C_{m(0)}$: concentrations of trace element in fractionated melt and initial melt, D : bulk K_d , F : fraction of melt remaining

^a Karmalkar et al. (2000), ^b Kinzler and Grove (1992), ^c GERM (2014), ^d Sheth et al. (2014)

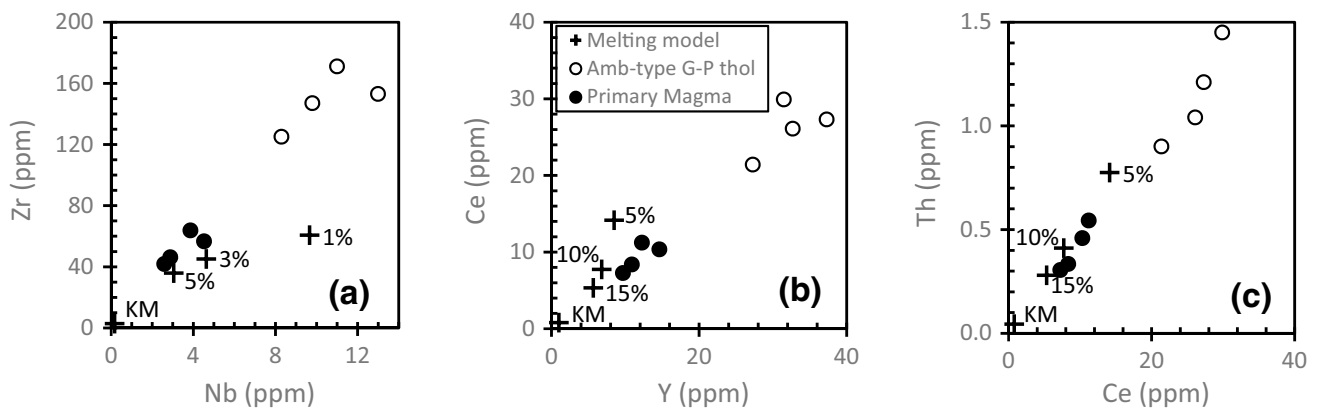


Fig. 11 Comparison of trace element contents of the Ambenali-type Ghatkopar–Powai tholeiitic dikes (MMD6, MMD12, MMD13, and MMD14, Sheth et al. 2014) and their primary magmas with different degrees of partial melts of the mantle below Kachchh (KM, Karmal-

kar et al. 2000). Note that the trace element contents of the primary magmas are consistent with their generation by 3–15 % batch partial melting of the Kachchh mantle

rif (Fig. 1a; Chandrasekharam et al. 2000). However, the Nd–Sr isotopic data do not indicate contamination by Si-rich, granitic upper crust in the Powai ankaramite (Sheth et al. 2014), precluding the origin of orthopyroxene through crustal assimilation. Another possibility for orthopyroxene formation is by low-temperature fractional crystallization of evolved tholeiitic liquids. Experiments at 1 bar indicate

that when a tholeiitic liquid saturated with Ol + Pl + Cpx cools, it may react with olivine at two different invariant points to produce either augite + pigeonite (Pig) or orthopyroxene + pigeonite (Grove and Baker 1984):



Pigeonite is minor or absent at higher pressures, where only one reaction, $\text{Ol} + \text{liq} = \text{Opx} + \text{Aug} + \text{Pl}$, is relevant (e.g., 5 kb experiments of Takahashi and Kushiro 1983, see Grove and Baker 1984). If the liquid is exhausted during this reaction, a cumulate rock consisting of $\text{Ol} + \text{Pl} + \text{Aug} + \text{Opx}$ will be created. On the other hand, if olivine is exhausted, the mafic crystals ($\text{Opx} + \text{Aug}$) may settle at the bottom of the magma pool, whereas the plagioclase may segregate toward the top due to its buoyancy in the Fe-rich tholeiitic liquid (Campbell et al. 1978). More likely, partially completed reactions will create an $\text{Ol} + \text{Aug} + \text{Opx}$ cumulate pile on the floor of the magma pool. When a new, relatively primitive and hot tholeiitic melt in equilibrium with only Ol , $\text{Ol} + \text{Pl}$, or $\text{Ol} + \text{Pl} + \text{Cpx}$ (depending on the extent of evolution), but not with Opx , comes in contact with the cumulate pile, the $\text{Opx} + \text{Aug} \pm \text{Pl}$ will react to form $\text{Ol} + \text{melt}$ through the above reactions operating in reverse. These melting reactions will end once the available plagioclase in the cumulate pile is consumed. Since the amount of plagioclase was probably low in the cumulate pile, as most of it presumably had separated during crystallization of the earlier magma, large-scale melting of the cumulate pile may not have occurred. The resulting liquid will subsequently cool and precipitate new $\text{Ol} + \text{Pl}$ or $\text{Ol} + \text{Pl} + \text{Cpx}$, and the new clinopyroxene may envelop the partially dissolved orthopyroxene crystals. The resorbed margins of the orthopyroxene indicating melt-crystal reaction, its exclusive occurrence within augite (Fig. 4a), the Fe–Mg disequilibrium between the cores of the large crystals and the groundmass, and sharp compositional changes in the outer parts of the large olivine and augite crystals indicate that orthopyroxene in the Powai ankaramite originated along with olivine and augite in an earlier formed cumulate pile by the above mechanism.

We reconstructed the composition of the liquid ($\text{GM}_{\text{liq(c)}}$) that intruded the cumulate pile by first adding back its crystallization products (i.e., outer parts of the large crystals and the overgrowths) to the groundmass (GM) and then subtracting orthopyroxene from the resulting liquid (GM_{liq}). Although augite and plagioclase were probably also assimilated along with orthopyroxene by $\text{GM}_{\text{liq(c)}}$, only resorbed orthopyroxene can be observed in the ankaramite. Resorbed cores may be obscured by oscillatory zoning in the augite. The original compositions, proportions and melting modes of olivine, orthopyroxene, augite, and plagioclase in the cumulate pile cannot be determined. However, we assume that the plagioclase content was low, and large-scale melting of the cumulate pile did not occur (see above). Thus, correcting for only orthopyroxene assimilation results in a reasonable approximation of $\text{GM}_{\text{liq(c)}}$ that shows multiple saturation at ~6 kb in the pseudoternary plots (Fig. 7). The estimated $\text{GM}_{\text{liq(c)}}$ composition is in equilibrium with $\text{Fo}_{\sim 79}$ olivine, augite of $\text{Mg\#} \sim 83$, and orthopyroxene of $\text{Mg\#} \sim 81$ (Table 5), which are similar to

the outer core or average compositions of the large crystals in the ankaramite (Fig. 5, Table 3). However, the evidence of orthopyroxene dissolution and disequilibrium of the inner core of olivine (Fo_{84}) with $\text{GM}_{\text{liq(c)}}$ indicate that $\text{GM}_{\text{liq(c)}}$ is not parental to the large crystals, and the outer cores of olivine probably equilibrated with $\text{GM}_{\text{liq(c)}}$ through Fe–Mg exchange. Thus, the estimated $\text{GM}_{\text{liq(c)}}$ composition fits well with our model of partial assimilation of the cumulate pile by an intruding melt.

The origin of the Powai ankaramite can thus be broadly summarized as follows: (a) An assemblage of $\text{Ol} + \text{Aug} + \text{Opx} \pm \text{Pl}$ existed in the form of a cumulate pile left over from crystallization of earlier tholeiitic magma, (b) a relatively primitive liquid ($\text{GM}_{\text{liq(c)}}$) intruded the cumulate pile at ~6 kb and ~1230 °C (Fig. 7, Table 5) and partially dissolved the preexisting $\text{Aug} + \text{Opx} \pm \text{Pl}$, forming a slurry of the left-over crystals and a liquid with assimilated crystals (GM_{liq}), and (c) the GM_{liq} liquid subsequently evolved by precipitating $\text{Ol} + \text{Pl} + \text{Aug}$ to form the groundmass (GM) and the overgrowths on preexisting crystals.

The Deccan primary magmas

The primary magmas of all of the Ghatkopar–Powai tholeiites and the melt inclusion and groundmass-related liquids ($\text{MI}_{\text{liq(c)}}$, $\text{GM}_{\text{liq(c)}}$) plot in the basalt field of the total alkali–silica diagram (Fig. 8). They contain 48–50 wt% SiO_2 , 9.8–11.8 wt% MgO , and 7.3–7.9 wt% FeO , and their Mg\# ranges between 70 and 74. Thus, they are primitive tholeiitic basalts. Our calculations show that most of these primary magmas last equilibrated at pressures of 8–11 kb and temperatures of 1268–1311 °C (with uncertainties of ± 0.8 kb and ± 12 °C as suggested by Till et al. 2012) with spinel lherzolite. We have used the thermobarometric expressions for anhydrous liquids (Till et al. 2012) in these calculations. Although we measured ~3.6 wt% H_2O in the groundmass of the ankaramite, most of this H_2O is in smectitic clay, a low-temperature alteration product with high H_2O content (~8 wt%, Table 4). Direct measurement of the primary H_2O is not possible because smectitic clay is abundant (~3.5 modal %, Table 2) in the groundmass. The pre-eruptive H_2O contents of primitive, olivine-hosted melt inclusions in continental flood basalts are very low (e.g., <0.25 wt% for the Siberian Traps, Sobolev et al. 2009), and the same is probably true for the Deccan primary magmas. According to Till et al.'s (2012) formulations, 1 wt% H_2O in the melt will reduce its temperature by ~27 °C and increase its pressure by ~0.2 kb. Thus, in the presence of ~1 wt% H_2O in the melts, the temperatures may be slightly lower than estimated in this study, whereas the departure from the estimated pressures will be within the quoted uncertainty.

We also performed similar thermobarometric and compositional calculations on an average Ambenali tholeiite and an average Mahabaleshwar tholeiite (Beane et al. 1986; Lightfoot et al. 1990) that plot on their respective 1 bar Ol + Pl + Cpx saturation points (Fig. 10). The compositions of the spinel lherzolite-equilibrated primary magmas of these tholeiites (48–49 wt% SiO₂, 10.5–10.9 wt% MgO, 7.2–7.5 wt% FeO, Mg# 71–73) are very similar to the primary magmas of the Powai ankaramite and Ghatkopar–Powai tholeiites (Table 5). The conditions at which these primary magmas were last equilibrated with mantle are 8–13 kb and 1272–1332 °C for the Ambenali and 9–10 kb and 1282–1294 °C for the Mahabaleshwar (Fig. 10, Table 5). Thus, most of the primary magmas of the Powai ankaramite and the Ghatkopar–Powai tholeiites, and the voluminous Ambenali and Mahabaleshwar tholeiites (with combined thickness of 780 m, Table 1) last equilibrated with mantle at similar P–T conditions. This is in agreement with the geochemical and isotopic similarities noted by Sheth et al. (2014) between the Powai ankaramite and Ghatkopar–Powai tholeiites and the Mahabaleshwar–Ambenali tholeiites.

Using an average density of 2.7 g/cm³ for continental crust, we calculate that the tholeiitic primary magmas of the Powai ankaramite and the Ghatkopar–Powai tholeiites last equilibrated with mantle at depths of 30–42 km (± 3 km). The 13-kb upper limit of pressure estimated for the Ambenali primary magma indicates that they equilibrated with mantle at depths up to 49 km (± 3 km). Our depth estimates (30–49 km) overlap with those of Sen (1988, 35–45 km) based on a comparison between the compositions of primitive Deccan tholeiites and experimental partial melts. However, our calculated primary magma compositions are significantly lower in FeO and have higher Mg# than Sen's (1988) estimates. In an MgO versus FeO plot, our calculated primary magma compositions do not indicate partial melting of Fe-rich peridotite postulated by Sen (1995) (Fig. 12). The picritic Ambenali primary magma compositions interpreted as parental to the Ambenali tholeiites by Sen (1995) plot near the garnet lherzolite multiple saturation point at 25 kb in the Ol–Pl–Cpx pseudoternary diagram projected from quartz (Fig. 13a), but they do not plot near any of the multiple saturation points in the Ol–Cpx–Qz diagram projected from plagioclase (Fig. 13b). Thus, Sen's (1995) estimated picritic magmas parental to the Ambenali tholeiites may not be primary magmas. By comparison, our estimated primary magmas of the Ambenali tholeiites plot on the 8- to 13-kb spinel lherzolite saturation points and are primitive tholeiitic basalts with <11 wt% MgO. Nevertheless, our estimate of the degree of mantle melting (≤ 15 %) to produce the Ambenali-type Ghatkopar–Powai tholeiites is comparable to Sen's (1995) estimate (15–18 %) for the Deccan primary magmas.

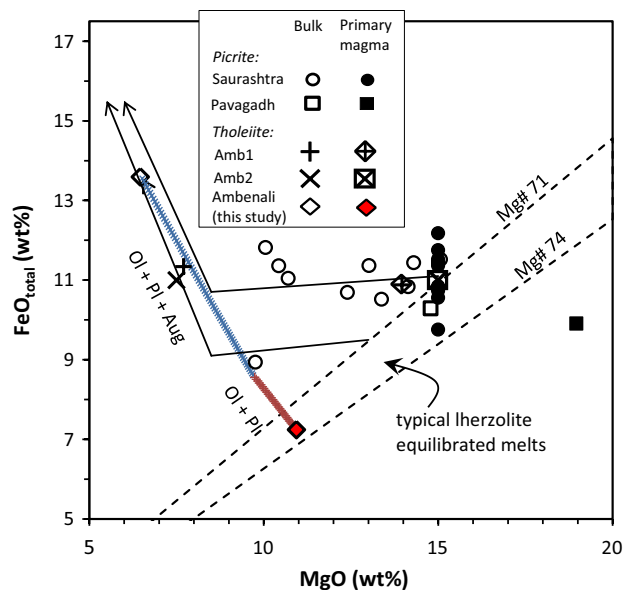


Fig. 12 MgO versus FeO_{total} plot showing the fractional crystallization path for an average Ambenali tholeiite (Beane et al. 1986; Lightfoot et al. 1990) calculated in this study (brown and blue crosses), compared with the calculated paths for Ambenali tholeiites in Sen (1995) (solid lines). The dashed lines represent the contours for the typical Mg# range (71–74) in melts of mantle peridotites. The compositions of Ambenali tholeiite, Amb1 and Amb2, are from Sen (1995), the Pavagadh picrite is from Sen and Chandrasekharam (2011), and the Saurashtra picrites are from Melluso et al. (1995). Note that the Ambenali primary magma calculated in this study is a Mg-rich tholeiite, whereas the compositions calculated and interpreted as Ambenali primary magmas by Sen (1995) are picritic and higher in Fe

Like the picritic Ambenali primary magma compositions estimated by Sen (1995), many of Melluso et al.'s (1995) estimated primary magma compositions for the Saurashtra–Gujarat picrites also plot near the 25-kb garnet lherzolite multiple saturation point in the Ol–Pl–Cpx diagram (Fig. 13a). In the Ol–Cpx–Qz diagram, they plot at normative Cpx values lower than the multiple saturation points and near the ~14 kb Ol + Opx saturation boundary (cf. Grove et al. 2013) (Fig. 13b). These magmas may have originated through melting of garnet lherzolite at ~25 kb (~80 km depth) and then equilibrated with harzburgite at shallower depths as proposed for the Hawaiian alkali basalts by Grove et al. (2013). Some other estimated Saurashtra–Gujarat primary magmas (Melluso et al. 1995) including the proposed primary magma of the Pavagadh (Fig. 1a) picrite (Sen and Chandrasekharam 2011) plot at higher Cpx values than the garnet lherzolite multiple saturation points in the Ol–Pl–Cpx diagram (Fig. 13a) and show silica undersaturation in the Ol–Cpx–Qz diagram (Fig. 13b). The proposed Pavagadh primary magma (Sen and Chandrasekharam 2011) is more silica undersaturated than the spinel lherzolite multiple saturation points

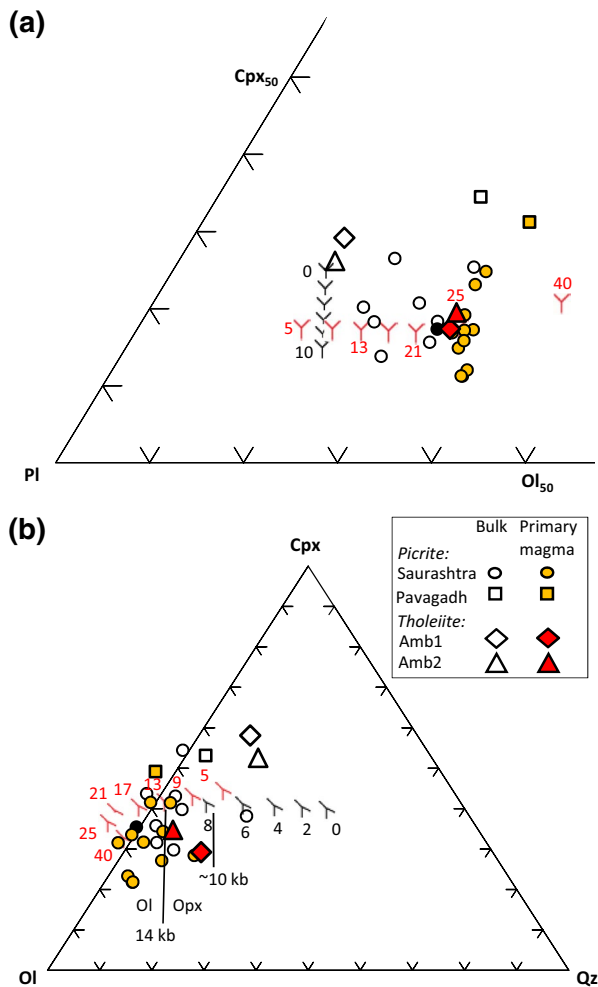


Fig. 13 **a** Ol-Pl-Cpx and **b** Ol-Cpx-Qz pseudoternary diagrams with Deccan volcanic rocks and compositions calculated and interpreted as their primary magmas in other studies, plotted as in Fig. 7 (Saurashtra picrites: Melluso et al. 1995, Pavagadh picrite: Sen and Chandrasekharam 2011, Ambenali tholeiites and their picritic parents: Sen 1995). The multiple-phase saturation boundaries are for the composition interpreted as the primary magma of picrite sample #57 (filled black circle, Melluso et al. 1995) at different pressures (black: 0.001–10 kb in 2-kb interval for plagioclase lherzolite; red: 5–21 kb in 4-kb interval for spinel lherzolite, and 25 and 40 kb using the expressions of Grove et al. 2013 for garnet lherzolite). The picrite #57 composition is chosen because it plots closest to its 25-kb multiple saturation points in both projections. The Ol-Opx saturation boundaries are as in Grove et al. (2013)

(Fig. 13b). Grove et al. (2013) conclude that such characteristics may indicate melting of a non-lherzolitic mantle source such as olivine pyroxenite, and Melluso et al. (1995) in fact inferred a clinopyroxene-rich source for the Saurashtra high-Ti picrites. Therefore, although the data show a large scatter in Fig. 13, origin of the Saurashtra-Gujarat picrites from a pyroxenite-like mantle source, or from a garnet lherzolite mantle source followed by equilibration with harzburgite, cannot be ruled out. The primary

magmas of the Saurashtra picrites (1430–1468 °C, Melluso et al. 1995) and the Pavagadh picrite (~1550 °C, Sen and Chandrasekharam 2011) yield much higher mantle potential temperatures than calculated in this study for the final equilibration of the primary magmas of the majority of the Deccan tholeiites (~1268–1332 °C). The different results probably reflect both mineralogical and temperature differences in the Deccan source mantle, besides melting and melt segregation at variable depths. However, our calculations indicate that the primary magmas of the bulk of the Deccan tholeiites were not anomalously hot.

A seismological study (Mohan and Ravi Kumar 2004) indicates that the crust immediately east and north of the Mumbai area is felsic to intermediate in composition and has a thickness of 36–41 km (± 2 km), typical of normal continental crust. Our depth estimates of 30–49 km (± 3 km) for the equilibration of the Deccan tholeiitic primary magmas overlap with the seismically constrained depths of the Moho, except for our minimum depth estimate of 30 ± 3 km, which is 6 km shallower than the minimum Moho depth. This may indicate that the Moho was shallower (i.e., the crust was extended and thinned at the time of active Deccan magmatism) than the present-day Moho. Alternatively, there was localized mantle upwelling into a thermally eroded, hot and ductile, lower crust. The latter scenario is consistent with the Nd-Sr isotopic ratios and some trace element characteristics of the Powai ankaramite and the Ghatkopar-Powai tholeiites that closely mimic those of the Mahabaleshwar tholeiites, for which a lower crustal contaminant has been previously postulated (Mahoney et al. 1982; Bhattacharya et al. 2013). Several tholeiitic dikes from Borlai-Korlai and elsewhere on the western Indian coast (Fig. 1b) with trace element compositions similar to the Mahabaleshwar tholeiites have also been interpreted as products of lower crustal contamination (Dessai et al. 2008; Vanderkluyzen et al. 2011; see Fig. 4 of Sheth et al. 2014). Xenoliths of mafic and felsic granulites representing such lower crust, along with crust-mantle transitional pyroxenites and websterites, are found in lamprophyre dikes at Murud-Janjira, south of Mumbai (Fig. 1b, Dessai et al. 2004).

Evolution of the Deccan tholeiitic primary magmas

The primary magmas of the Powai ankaramite and the Ghatkopar-Powai tholeiites equilibrated with the mantle at the Moho or somewhat shallower depths, ascended through the crust, and underwent olivine gabbro fractionation in upper crustal magma chambers. Using phase equilibrium relations predicted with the equations of Till et al. (2012), the highest estimated pressures in these chambers are ~6 kb as constrained from the $GM_{liq(c)}$ liquids in the ankaramite that reacted with the cumulate pile, and the

Fo_{77–82}-equilibrated parental liquids with Mg# 50–58 of two tholeiites, MMD12 and MMD14 (Table 5). The temperatures of these liquids were ~1230–1260 °C (Table 5). The parental liquids of MMD12 and MMD14 crystallized in the uppermost crust, as did the other evolved liquids ($M_{liq(c)}$ in the ankaramite and the Ghatkopar–Powai tholeiites) that show equilibrium pressures of 1 bar to 2 kb, and temperatures of ~1160–1220 °C (Table 5). Villiger et al.'s (2007) equation yields similar or slightly higher pressures (~6.9 kb for $G_{M_{liq(c)}}$ in the ankaramite, 5.7 kb for the parent of MMD14, and <3.8 kb for the Ghatkopar–Powai tholeiitic liquids; Table 5). We thus estimate that the upper crustal magma chambers were at ≤ 23 km depths (≤ 6 kb pressures).

A prominent gravity anomaly (+100 mgals and 100 km \times 100 km in lateral extent) over the Mumbai area has been known for long and interpreted as a large mafic intrusion (Glennie 1951) or a magma chamber of olivine gabbro composition (Takin 1966). Gravity modeling indicates large high-density intrusive bodies or magma chambers reaching mid-crustal depths (~18 km) below the Mumbai area (Bhattacharji et al. 2004). The Ghatkopar–Powai tholeiites probably evolved in these magma chambers, where mafic cumulate piles were formed by the fractionation of tholeiitic melts, some of which were sufficiently evolved to precipitate orthopyroxene. Intrusion of a batch of tholeiitic magma into such a cumulate pile, dissolution of orthopyroxene, and subsequent crystallization of olivine, plagioclase, and augite produced the Powai ankaramite.

Conclusions

We have shown through thermobarometric calculations that most of the Deccan primary magmas of the Powai ankaramite and the Ghatkopar–Powai tholeiites in the Mumbai area, as well as those of the voluminous Ambenali and Mahabaleshwar Formation tholeiites in the Western Ghats sequence, are primitive tholeiites (MgO 8.74–11.77 wt%, Mg# 70–74; not picrites as concluded in previous studies) that last equilibrated with mantle peridotite at temperatures of 1268–1332 °C (± 12 °C) and pressures of 8.0–13.0 kb (± 0.8 kb). The estimated pressures correspond with depths of 30–49 km (± 3 km) that overlap with the present-day seismically constrained Moho depths of 36–41 km (± 2 km) below Mumbai and nearby areas. The primary magmas originated by ≤ 15 % batch melting of the mantle, ascended through the crust, and pooled and evolved in magma chambers at depths ≤ 23 km. Such chambers have been identified previously from geophysical modeling. The primary magmas underwent olivine gabbro fractionation to produce mafic cumulate piles (Ol + Cpx + Opx) at the bottom of the magma chambers, with plagioclase probably

separating due to its buoyancy. Later batches of tholeiitic magmas would pierce these cumulate piles, leading to the formation of cumulate rocks such as the Powai ankaramite, in which we have identified dissolution of orthopyroxene and subsequent crystallization of augite, olivine, and plagioclase. The tholeiitic primary magmas of the Powai ankaramite, the Ghatkopar–Powai tholeiites, and the voluminous Ambenali and Mahabaleshwar tholeiites of the Western Ghats last equilibrated with spinel lherzolite mantle that was neither Fe rich nor anomalously hot.

Acknowledgments We gratefully appreciate the detailed and constructive comments of the journal reviewers Jean Bédard, Fanny Sorbadere and an anonymous reviewer that greatly improved the presentation of this paper. Comments and editorial help of Othmar Müntener and informal discussions with Tim Grove are also greatly appreciated. Tim's MORBFRAC program was used to perform the reverse fractional crystallization calculations.

References

- Armstrong JT (1995) CITZAF—a package for correction programs for the quantitative electron microbeam X-ray analysis of thick polished materials, thin-films and particles. *Microbeam Anal* 4:177–200
- Beane JE, Hooper PR (1988) A note on the picrite basalts of the Western Ghats, Deccan Traps, India. In: Subbarao KV (ed) *Deccan flood basalts*, Mem Geol Soc India 10, Bangalore, pp 117–133
- Beane JE, Turner CA, Hooper PR, Subbarao KV, Walsh JN (1986) Stratigraphy, composition and form of the Deccan basalts, Western Ghats, India. *Bull Volcanol* 48:61–83
- Bédard JH (2007) Trace element partitioning coefficients between silicate melts and orthopyroxene: parameterizations of D variations. *Chem Geol* 244:263–303
- Bédard JH (2010) Parameterization of the Fe = Mg exchange coefficient (K_d) between clinopyroxene and silicate melts. *Chem Geol* 274:169–176
- Bhattacharji S, Chatterjee N, Wampler JM, Nayak PN, Deshmukh SS (1996) Indian intraplate and continental margin rifting, lithospheric extension and mantle upwelling in Deccan flood basalt volcanism near K/T boundary: evidence from mafic dike swarms. *J Geol* 104:379–398
- Bhattacharji S, Sharma R, Chatterjee N (2004) Two and three-dimensional gravity modeling along western continental margin and intraplate Narmada-Tapti rifts: its relevance to Deccan flood basalt volcanism. In: Sheth HC, Pande K (eds) *Magmatism in India through time*, Proc Indian Acad Sci (Earth Planet Sci) 113/4:771–784
- Bhattacharya SK, Ma GSK, Matsuhisa Y (2013) Oxygen isotope evidence for crustal contamination in Deccan basalts. *Chem Erde* 73:105–112
- Campbell IH, Roeder PL, Dixon JM (1978) Plagioclase buoyancy in basaltic liquids as determined with a centrifuge furnace. *Contrib Mineral Petrol* 67:369–377
- Chandrasekharam D, Vaselli O, Sheth HC, Keshav S (2000) Petrogenetic significance of ferro-enstatite orthopyroxene in basaltic dikes from the Tapi rift, Deccan flood basalt province, India. *Earth Planet Sci Lett* 179:469–476
- Cohen TH, Sen G (1994) Fractionation and ascent of Deccan trap magmas: an experimental study at 6 kilobar pressure. In: Subbarao KV (ed) *Volcanism*, Wiley Eastern, pp 173–186

- Courtier AM, Jackson MG, Lawrence JF, Wang Z, Lee C-TA, Halama R, Warren J, Workman R, Xu W, Hirschmann MM, Larson AM, Hart SR, Stixrude L, Lithgow-Bertelloni C, Chen W-P (2007) Correlation of seismic and petrologic thermometers suggest deep thermal anomalies beneath hot spots. *Earth Planet Sci Lett* 264:308–316
- Cox K (1980) A model for flood basalt volcanism. *J Petrol* 21:629–650
- Cox KG, Hawkesworth CJ (1985) Geochemical stratigraphy of the Deccan traps at Mahabaleshwar, Western Ghats, India, with implications for open system magmatic processes. *J Petrol* 26:355–377
- Cucciniello C, Choudhary AK, Zanetti A, Sheth HC, Vichare S, Pereira R (2014) Mineralogy, geochemistry and petrogenesis of the Khopoli mafic intrusion, Deccan Traps, India. *Mineral Petrol* 108:333–351
- Dessai AG, Marckwick A, Vaselli O, Downes H (2004) Granulite and pyroxenite xenoliths from the Deccan Trap: insight into the nature and composition of the lower lithosphere beneath cratonic India. *Lithos* 78:263–290
- Dessai AG, Downes H, López-Moro FJ, López-Plaza M (2008) Lower crustal contamination of Deccan Traps magmas: evidence from tholeiitic dykes and granulitic xenoliths from western India. *Mineral Petrol* 93:243–272
- Falloon TJ, Green DH, O'Neill HSC, Hibberson WO (1997) Experimental tests of low degree peridotite partial melt compositions: implications for the nature of anhydrous near-solidus peridotite melts at 1 GPa. *Earth Planet Sci Lett* 152:149–162
- Falloon TJ, Danyushevsky LV, Green DH (2001) Peridotite melting at 1 GPa: reversal experiments on partial melt compositions produced by peridotite-basalt sandwich experiments. *J Petrol* 42:2363–2390
- Farnetani C, Richards M, Ghiorso M (1996) Petrological models of magma evolution and deep crustal structure beneath hotspots and flood basalt provinces. *Earth Planet Sci Lett* 143:81–94
- Gaetani GA, Grove TL (1998) The influence of water on melting of mantle peridotite. *Contrib Mineral Petrol* 131:323–346
- GERM (2014) Geochemical earth reference model partition coefficient (Kd) database. *Earth Ref. org.* <http://earthref.org/KDD/>. Accessed July 2014
- Glennie EA (1951) Density or geological corrections to gravity anomalies for the Deccan trap areas in India. *R Astron Soc Geophys Suppl* 6:179–193
- Green DH, Falloon TJ, Eggins SM, Yaxley GM (2001) Primary magmas and mantle temperatures. *Eur J Mineral* 13:437–451
- Grove TL (1993) Corrections to expressions for calculating mineral components in “Origin of calc-alkaline series lavas at Medicine Lake volcano by fractionation, assimilation and mixing” and “Experimental petrology of normal MORB near the Kane Fracture Zone: 22°–25°N, mid-Atlantic ridge”. *Contrib Mineral Petrol* 114:422–424
- Grove TL, Baker MB (1984) Phase equilibrium controls on the tholeiitic versus calc-alkaline differentiation trends. *J Geophys Res* 89(B5):3253–3274
- Grove TL, Kinzler RJ, Bryan WB (1992) Fractionation of mid-ocean ridge basalt (MORB). In: Phipps-Morgan J, Blackman DK, Sinton JM (eds) *Mantle flow and melt generation at mid-oceanic ridges*, Am Geophys Monograph 71, Am Geophys Union, Washington DC, pp 281–310
- Grove TL, Holbig ES, Barr JA, Till CB, Krawczynski MJ (2013) Melts of garnet lherzolite: experiments, models and comparison to melts of pyroxenite and carbonated lherzolite. *Contrib Mineral Petrol* 166(3):887–910
- Herzberg C (2004) Partial crystallization of mid-ocean ridge basalts in the crust and mantle. *J Petrol* 45:2389–2405
- Hirose K, Kushiro I (1993) Partial melting of dry peridotites at high pressures: determination of compositions of melts segregated from peridotite using aggregates of diamond. *Earth Planet Sci Lett* 114:477–489
- Karmalkar NR, Griffin WL, O'Reilly SY (2000) Ultramafic xenoliths from Kutch, northwest India: plume-related mantle samples? *Intern Geol Rev* 42(5):416–444
- Khadri SFR, Subbarao KV, Hooper PR, Walsh JN (1988) Stratigraphy of Thakurvadi formation, western Deccan basalt province, India. In: Subbarao KV (ed) *Deccan flood basalts*, Geol Soc India Mem 10, pp 281–304
- Kinzler RJ (1997) Melting of mantle peridotite at pressures approaching the spinel to garnet transition: application to mid-ocean ridge basalt petrogenesis. *J Geophys Res* 102:853–874
- Kinzler RJ, Grove TL (1992) Primary magmas of mid-ocean ridge basalts. 1 Experiments and methods. *J Geophys Res* 97:6885–6906
- Klein E, Langmuir CH (1987) Global correlations of ocean ridge basalt chemistry with axial depth and crustal thickness. *J Geophys Res* 92:8089–8115
- Krishnamacharlu T (1972) Petrology of the picrodolerites from the Dedan cluster, Gujarat. *J Geol Soc India* 13:262–272
- Krishnamurthy P, Cox KG (1977) Picrite basalts and related lavas from the Deccan Traps of western India. *Contrib Mineral Petrol* 62:53–75
- Krishnamurthy P, Gopalan K, Macdougall JD (2000) Olivine compositions in picrite basalts and the Deccan volcanic cycle. *J Petrol* 41:1057–1069
- Laporte D, Toplis MJ, Seyler M, Devidal J-L (2004) A new experimental technique for extracting liquids from peridotite at very low degrees of melting: application to partial melting of depleted peridotite. *Contrib Mineral Petrol* 146:463–484
- Laubier M, Grove TL, Langmuir CH (2010) Laser ICP-MS study of trace element partitioning between olivine, plagioclase, orthopyroxene and melt. *Am Geophys Union Fall Meeting*, San Francisco, CA, USA, abstract #V43A-2338
- Le Bas MJ (2000) IUGS re-classification of the high-Mg and picritic volcanic rocks. *J Petrol* 41:1467–1470
- Le Bas MJ, Le Maitre RW, Streckeisen A, Zanettin B (1986) A chemical classification of volcanic rocks based on the total alkali-silica diagram. *J Petrol* 27:745–750
- Lightfoot PC, Hawkesworth CJ (1988) Origin of Deccan Trap lavas: evidence from combined trace element and Sr-, Nd- and Pb- isotope data. *Earth Planet Sci Lett* 91:89–104
- Lightfoot PC, Hawkesworth CJ, Devey CW, Rogers NW, van Calsteren PWC (1990) Source and differentiation of Deccan Trap lavas: implications of geochemical and mineral chemical variations. *J Petrol* 31:1165–1200
- Longhi J (2002) Some phase equilibrium systematics of lherzolite melting: I. *Geochem Geophys Geosyst* 3: art no-1020
- Macdonald GA, Katsura T (1964) Chemical composition of Hawaiian lavas. *J Petrol* 5:82–133
- Mahoney JJ, Macdougall JD, Lugmair GW, Murali AV, Sankar Das M, Gopalan K (1982) Origin of the Deccan trap flows at Mahabaleshwar inferred from Nd and Sr isotopic and chemical evidence. *Earth Planet Sci Lett* 60:47–60
- Melluso L, Beccaluva L, Brotzu P, Gregnanin A, Gupta AK, Morbidelli L, Traversa G (1995) Constraints on the mantle sources of the Deccan Traps from the petrology and geochemistry of Basalts of Gujarat state, western India. *J Petrol* 36:1393–1432
- Melluso L, Mahoney JJ, Dallai L (2006) Mantle sources and crustal input as recorded in high-Mg Deccan Traps basalts of Gujarat (India). *Lithos* 89:259–274
- Middlemost EAK (1989) Iron oxidation ratios, norms and the classification of volcanic rocks. *Chem Geol* 77:19–26
- Mohan G, Ravi Kumar M (2004) Seismological constraints on the structure and composition of western Deccan volcanic province from converted phases. *Geophys Res Lett* 31:L02601
- Morgan Z, Liang Y, Kelemen P (2008) Significance of the concentration gradients associated with dunite bodies in the Josephine and

- Trinity ophiolites. *Geochim Geophys Geosyst* 9:Q07025. doi:10.1029/2008GC001954
- Peng ZX, Mahoney J, Hooper P, Harris C, Beane J (1994) A role for lower continental crust in flood basalt genesis? Isotopic and incompatible element study of the lower six formations of the western Deccan Traps. *Geochim Cosmochim Acta* 58:267–288
- Pickering-Witter J, Johnston AD (2000) The effects of variable bulk composition on the melting systematics of fertile peridotitic assemblages. *Contrib Mineral Petrol* 140:190–211
- Robinson JAC, Wood BJ, Blundy JD (1998) The beginning of melting of fertile and depleted peridotite at 1.5 GPa. *Earth Planet Sci Lett* 155:97–111
- Roeder PL, Emslie RF (1970) Olivine liquid equilibrium. *Contrib Mineral Petrol* 29:275–289
- Sano T, Fujii T, Deshmukh SS, Fukuoka T, Aramaki S (2001) Differentiation processes of Deccan Trap basalts: contribution from geochemistry and experimental petrology. *J Petrol* 42:2175–2195
- Schiano P (2003) Primitive mantle magmas recorded as silicate melt inclusions in igneous minerals. *Earth Sci Rev* 63:121–144
- Sen G (1988) Possible depth of origin of primary Deccan tholeiite magma. In: Subbarao KV (ed) *Deccan flood basalts*. Mem Geol Soc India 10, Bangalore, pp 35–51
- Sen G (1995) A simple petrologic model for the generation of Deccan Trap magmas. *Intern Geol Rev* 37:825–850
- Sen G, Chandrasekharam D (2011) Deccan Traps flood basalt province: an evaluation of the thermomechanical plume model. In: Ray J, Sen G, Ghosh B (eds) *Topics in igneous petrology*. Springer, Berlin, pp 29–54
- Shaw DM (1970) Trace element fractionation during anatexis. *Geochim Cosmochim Acta* 34(2):237–243
- Sheth HC (1998) A reappraisal of the coastal Panvel flexure, Deccan Traps, as a listric-fault-controlled reverse drag structure. *Tectonophysics* 294:143–149
- Sheth HC, Melluso L (2008) The Mount Pavagadh volcanic suite, Deccan Traps: geochemical stratigraphy and magmatic evolution. *J Asian Earth Sci* 32:5–21
- Sheth HC, Pande K (2014) Geological and $^{40}\text{Ar}/^{39}\text{Ar}$ age constraints on late-stage Deccan rhyolitic volcanism, inter-volcanic sedimentation, and the Panvel flexure from the Dongri area, Mumbai. In: Sheth HC, Vanderkluysen L (eds) *Flood Basalts of Asia*, *J Asian Earth Sci* 84:167–175
- Sheth HC, Zellmer GF, Demonerova EI, Ivanov AV, Kumar R, Patel RK (2014) The Deccan tholeiite lavas and dykes of Ghatkopar-Powai area, Mumbai, Panvel flexure zone: geochemistry, stratigraphic status, and tectonic significance. In: Sheth HC, Vanderkluysen L (eds) *Flood Basalts of Asia*, *J Asian Earth Sci* 84:69–82
- Sobolev A, Krivolutsкая N, Kuzmin D (2009) Petrology of the parental melts and mantle sources of Siberian Trap magmatism. *Petrology* 17:253–286
- Subbarao KV, Hooper PR (1988) Reconnaissance map of the Deccan basalt group in the Western Ghats, India. In: Subbarao KV (ed) *Deccan flood basalts*, Geol Soc India Mem 10, enclosure
- Subbarao KV, Bodas MS, Hooper PR, Walsh JN (1988) Petrogenesis of Jawhar and Igatpuri formations, western Deccan basalt province, India. In: Subbarao KV (ed) *Deccan flood basalts*, Geol Soc India Mem 10:253–280
- Takahashi E, Kushiro I (1983) Melting of a dry peridotite at high pressures and basalt magma genesis. *Am Mineral* 68:859–879
- Takahashi E, Nakajima K, Wright TL (1998) Origin of the Columbia Rivers basalts: melting model of a heterogeneous plume head. *Earth Planet Sci Lett* 162:63–80
- Takin M (1966) An interpretation of the positive gravity anomaly over Bombay on the west coast of India. *J Astron Soc Geophys Suppl* 11:527–537
- Thompson RN (1975) Primary basalts and magma genesis II. Snake River plain, Idaho, USA. *Contrib Mineral Petrol* 52:213–232
- Till CB, Grove TL, Krawczynski MJ (2012) A melting model for variably depleted and enriched lherzolite in the plagioclase and spinel stability fields. *J Geophys Res* 117:B06206
- Till CB, Grove TL, Carlson RW, Fouch MJ, Donnelly-Nolan JM, Wagner LS, Hart WK (2013) Depths and temperatures of <10.5 Ma mantle melting and the lithosphere-asthenosphere boundary below southern Oregon and northern California. *Geochim Geophys Geosyst* 14:864–879. doi:10.1002/ggge.20070
- Tormey DR, Grove TL, Bryan WB (1987) Experimental petrology of normal MORB near the Kane Fracture Zone: 22–25°N, mid-Atlantic Ridge. *Contrib Mineral Petrol* 96:121–139
- Vanderkluysen L, Mahoney JJ, Hooper PR, Sheth HC, Ray R (2011) The feeder system of the Deccan Traps (India): insights from dike geochemistry. *J Petrol* 52:315–343
- Villiger S, Müntener O, Ulmer P (2007) Crystallization pressures of mid-ocean ridge basalts derived from major element variations of glasses from equilibrium and fractional crystallization experiments. *J Geophys Res* 112:B01202
- Wadia DN (1975) *Geology of India*, 4th edn. Tata McGraw-Hill, New Delhi 508 p
- Wasylenki LE, Baker MB, Kent AJR, Stolper EM (2003) Near-solidus melting of the shallow upper mantle: partial melting experiments on depleted peridotite. *J Petrol* 44:1163–1191
- West WD (1958) The petrography and petrogenesis of forty eight flows of Deccan Trap penetrated by borings in western India. *Trans Nat Inst Sci India* 4:1–56
- Yang H-J, Kinzler RJ, Grove TL (1996) Experiments and models of anhydrous, basaltic olivine-plagioclase-augite saturated melts from 0.001 to 10 kbar. *Contrib Mineral Petrol* 124:1–18
- Yoder HS, Tilley CE (1962) Origin of basalt magmas; an experimental study of natural and synthetic rock systems. *J Petrol* 3(3):342–529